AN INVESTIGATION OF THE EFFECTS OF ACCELERATION AND STRAND LENGTH ON POST-FIRE RESIDUE OF ALUMINIZED PROPELLANTS

by

David Eugene Cowles

[redacted]

United States Naval Postgraduate School

THESIS

AN INVESTIGATION OF THE EFFECTS OF ACCELERATION AND STRAND LENGTH ON POST-FIRE RESIDUE OF ALUMINIZED PROPELLANTS

by

David Eugene Cowles

[redacted]

An Investigation of the Effects of Acceleration and Strand Length on Post-Fire Residue of Aluminized Propellants

by

David Eugene Cowles
Lieutenant Commander, United States Navy
B.A.E., University of Virginia, 1960

Submitted in partial fulfillment of the
requirements for the degree of

MASTER OF SCIENCE IN AERONAUTICAL ENGINEERING

from the

NAVAL POSTGRADUATE SCHOOL
April 1970

ABSTRACT

Aluminized propellant strand lengths from one-quarter to two inches were burned at accelerations from zero to 1000g at a mean combustion pressure of 500 psia to study the effect of acceleration and strand length on burning rate augmentation. Propellant ammonium perchlorate oxidizer size and base burning rate were varied to investigate their effects. Each post-fire residue was photographically recorded and chemical analysis was performed by X-Ray powder diffraction.

Burning rate augmentation decreased and residue weight increased when the strand length was increased. Aluminum and aluminum oxide were identified at low accelerations independent of strand length; aluminum oxide was not detectable at high accelerations. Ammonium perchlorate size and base burning rate had little effect on the functional dependence of residue weight on burn time. The Crowe, et al., model was found to indicate the correct augmentation trend as a function of burn time if the time-history of the metallic agglomerates is known.

TABLE OF CONTENTS

LIST OF TABLES

LIST OF FIGURES

SYMBOLS AND ABBREVIATIONS

AP	Ammonium Perchlorate
cc	Cubic centimeter
g	Acceleration divided by gravitational constant
ips	Inches per second
mg	Milli-gram
μ	Microns
$\dot{r}$	Burning rate
$\dot{r}_o$	Base burning rate (0g)

ACKNOWLEDGEMENTS

The author gratefully acknowledges the guidance and many hours of counseling furnished by his thesis advisor, Dr. David W. Netzer. The encouragement and freedom of direction given the author is sincerely appreciated. Dr. Netzer's eagerness to insure that the author gained maximum benefit from the investigation, its evaluation and ultimate presentation was certainly without bound.

The author sincerely appreciates the many hours of complete sample preparation generously given by Mr. Edward Michelson. His cheerful assistance brightened many long, arduous data sessions.

The author also expresses his gratitude to Dr. John R. Clark who generously volunteered his time and advice on X-Ray powder diffraction. Without his help, this portion of the investigation could not have been completed.

Finally, the author acknowledges the encouragement and perseverance of his wife, Druscilla, whose understanding made this effort possible.

I. INTRODUCTION

Spin stabilized rockets have been observed to burn at significantly greater rates than under static conditions. This augmentation of the burning rate in the presence of an acceleration field directed towards the burning surface increases the chamber pressure and generally reduces the total impulse of the rocket. In order to optimize chamber strength, rocket nozzle contour, and other design criteria, the augmentation must be known throughout the acceleration ranges of the spinning rocket. Numerous investigations have been conducted and have recently been summarized by Netzer, et al., [Ref. 1].

The weight and form of molten residue on the burning surface have been shown to have a dominant effect on augmentation [Ref. 1]. Both the weight and form of the residue are strongly affected by propellant properties, the acceleration level, and the burn time.

There are three techniques most generally employed to study the behavior of the burning propellant. Cinematographic observations may be made of the propellant during the actual burning process. Excellent results were recently obtained by Willoughby, et al., using this procedure [Ref. 2]. Propellant samples may be extinguished at selected intervals during the burning process to analyze the propellant surface structure as a function of burn time. The third method is to burn strands of different lengths under the same environmental conditions. Post-fire analysis of the residue of different strand

lengths gives an active picture of the molten residue formation throughout the longest strand. It was this last technique that was employed in this investigation.

In the previous work of Netzer, et al., [Ref. 1] residue form was only roughly determined. This investigation included detailed photographs of the residue samples. Additionally, X-Ray powder diffraction patterns were made in an attempt to determine the residue composition. Hence this investigation extends the previous work to include both photographic and composition analysis of the residue.

The most promising analytical model for predicting the burning rate augmentation of metallized propellants has been proposed by Crowe, et al., [Ref. 3]. That investigation qualitatively analyzed the model's ability to correctly predict augmentation trends as a function of propellant properties, pressure, and acceleration. In order to apply the model, properties of the metallic globules (oblateness, size, and density) must be known. Further refinement of the model must include the dependence of these properties on propellant formulation, acceleration, pressure, and burn time. It was the purpose of this investigation to provide data on how particle oblateness, size, and density vary with acceleration and burn time.

II. METHOD OF INVESTIGATION

In order to investigate the effects of strand length (burn time), base burning rate, and ammonium perchlorate (AP) size on burning rate acceleration sensitivity, three propellant formulations were utilized. The propellant designations and their formulations are given in Table I.

N6 was selected as the reference propellant. Strand lengths of one-quarter, one-half, and one inch were investigated at selected accelerations from zero g to 1000g, and two-inch strands were studied at zero, 100, and 500g. This allowed a study of the effects of acceleration and strand length (burn time) on burning rate augmentation, post-fire residue weight, and post-fire residue composition.

Propellants N7 and N9 were utilized to investigate the effects of AP size and base burning rate, defined to be the burning rate at zero acceleration. Strand lengths of one-half inch and two inches were burned at zero, 100, and 500g for comparison to the similar tests of N6. Propellant N7 differed from N6 only in AP size and base burning rate; hence a comparison of these two propellants includes the effects of a change in both of these parameters. Propellant N9 was essentially the same as N7 except that it contained an iron oxide (Fe_2O_3) catalyst which increased the base burning rate.

Following each test where residue was observed, photographs of 1.8 magnification were taken of the residue in its inhibitor case (Fig. 4, 5, 6, 7, and 14). In isolated instances photographs were

taken of the residue after it had been removed from the case (Fig. 7). This permitted a study of both the upper and lower surfaces. Each residue was then weighed.

X-Ray diffraction powder tests were made on one residue at each acceleration level in a test series. In some cases at the lower acceleration levels, residue from two samples at the same acceleration were combined in order to obtain a powder sample of sufficient magnitude for the diffraction process. Because of the low residue weights of the one-quarter inch samples of N6, no X-Ray diffraction was attempted at this strand length.

For each strand burned there were, in effect, three sets of data representing the three dependent variables investigated: (1) burning rate and burning rate augmentation, (2) residue weight and physical appearance, and (3) chemical composition of the residue.

III. EXPERIMENTAL PROCEDURE

This investigation was conducted at the Naval Postgraduate School Rocket Test Facility. A centrifuge-mounted combustion bomb was employed to study the influence of acceleration on the burning of propellant strands. The test facility is discussed in detail in References 4 and 5.

The combustion bomb was mounted at a three-foot radius, which provided an approximately constant centripetal acceleration during the burning process. The largest variation of acceleration during a given test was less than six percent. All acceleration was directed normal and into the burning surface. All strand cross-sections were one-half by one-half inches, and strand lengths varied from one-quarter to two inches.

All tests were made at pressure settings intended to give a mean bomb pressure of 500 psi. The mean bomb pressure was the pressure initially set in the combustion bomb while it was static, plus the pressure rise due to acceleration, plus the mean pressure rise due to the burning of the propellant. The largest pressure variation from the mean bomb pressure was about five percent and is schematically shown in Fig. 1.

All four sides and the base of the propellant strand were rigidly inhibited with Selectron 5119 resin and "Garox" curing agent. During preliminary investigations, copper inserts were placed in the base to

quickly quench the propellant at burn-out. This procedure had no noticeable effect on propellant burn time, residue appearance, or residue weight and was not utilized for any strands discussed herein. The copper inserts actually produced an undesirable effect on preserving residue appearance. Normally the residue particles embed themselves into the inhibitor base and their as-burned positions are frozen. The copper permitted the particles to shift during photographic analysis.

The strand was ignited by a thin layer of a black powder-glue mixture placed across the propellant surface. The black powder, in turn, was ignited by a nichrome resistance wire adjacent to the propellant surface. Although the ignition current was adjusted so that the wire would not burn out, if burn-out did occur the location of the wire prevented it from falling onto the burning propellant.

The propellant was taped to a strand holder and sealed in the combustion bomb. The initial static pressure was set and the centrifuge was brought to the desired speed. The strand was ignited and a bomb pressure-time trace was recorded with a Visiograph recorder.

The pressure-time trace typically exhibited a pressure peak and fall-off followed by a steady pressure rise (Fig. 1). Burn-out was taken to be the sharp pressure drop after the steady burning process. Average burning rate was determined by dividing the known strand length by burn time measured from the pressure-time trace. The mean

pressure of the pressure-time trace was determined in order that the actual mean combustion bomb pressure during the burning process could be calculated.

Photographs were taken of all observed residues. Most residues were photographed while still in the inhibitor case. In order to provide adequate lighting, the walls of the case were cut through and removed about one-quarter to three-eighths of an inch above the residue peaks. A fine-tooth jeweler's saw was utilized to minimize vibrations in order to preserve the residue pieces in their original patterns.

All residue samples were covered by carbon fluff of varying thickness and compactness. This was removed from the residue surface by lightly blowing and brushing with a very soft bulb-type photographic lens brush.

A 35mm Nikon F camera was utilized with an f1.4 50mm lens mounted in the reversed position on two E_2 extension rings. Eastman Kodak TRI-X Pan Film was used, rated at 1200 ASA; it was developed in Acufine. Two photofloods 150 degrees apart, about ten inches from the subject, produced exposures at f16, varying from 1/125th to 1/500th of a second. The small exposure aperature was considered essential in order to achieve an acceptable depth of field. The lens arrangement utilized produced a magnification on the negative of 1.8. The one-half inch wide sample thus fills the shorter of the negative dimensions.

Powder X-Ray diffraction was performed utilizing a Philips X-Ray Diffraction Unit with a Mark III Data Control and Processor. A copper

target X-Ray tube was used and was operated at 45 kv and 37 ma. The counter receiving slit was 0.003 inches; no filter was used.

Each sample was ground into a fine powder utilizing a standard laboratory ceramic crucible. The powder was mounted on glass slides using vaseline jelly as the holding agent. A thin strip of vaseline was spread across the slide and the powder dusted onto it. The slide was tilted and tapped lightly to shed any excess powder. This excess was re-dusted onto the slide and the process was repeated until the vaseline area was completely covered. In an effort to avoid preferred crystal direction problems, at no time was the powder pressed into the vaseline. Generally, about 30 milligrams of residue were required in order to prepare a uniform sample.

Each specimen was scanned for two-theta angles from 30 to 80 degrees. The N6 one-half-inch and one-inch series were studied at a scanning rate of two degrees per minute, one-half-second time gate, and no pulse height analyzer. The remaining samples were scanned at a one-degree-per-minute scanning rate and a one-second time gate. Pulse height analyzer settings of 1.9 baseline and 4.1 window were required for the N9 residues in order to eliminate the severe fluorescence due to the apparent presence of iron atoms. A check of these settings on previous samples produced the same patterns with somewhat lower intensities.

The X-Ray diffraction system was standardized against a known sample of silicon powder (ser. #217) provided by North American Philips

Company. A two-theta error of about 0.3 degrees was detected throughout the range scanned. The data listed in the report reflect this correction. The intensity listed is the number of counts above the noise level of the scanning trace.

Aluminum and aluminum oxide (α-Al_2O_3) were anticipated in the residue and each powder pattern was first searched for the possibility of their presence. N9 residue powder patterns were additionally specifically searched for Fe_3O_4, Fe_2O_3 and iron. After any of these specific patterns were recognized, the strongest remaining angles were searched as described in Reference 6.

IV. EXPERIMENTAL RESULTS AND DISCUSSION

A. GENERAL DISCUSSION

The data are discussed in the following sequence: (1) the effect of acceleration on the reference propellant N6; (2) the results of variation in the strand length; (3) effects of simultaneous variation of AP size and base burning rate (a comparison of N6 and N7); (4) effect of AP size alone (a comparison of N6 and N9); and (5) effect of base burning rate alone (a comparison of N7 and N9).

The burning rate and residue weight data are presented in Table II. In addition, selected data are plotted, as appropriate, and are referred to in the following sections. The lines drawn on these plots do not represent any type of mathematical curve fitting; they are merely an aid in visualizing the data.

B. EFFECT OF ACCELERATION ON PROPELLANT N6

Increasing acceleration caused an increase in burning rate augmentation throughout the entire acceleration range investigated (Fig. 2). Augmentation increased rapidly from zero g to 300g. Above 300g the rate of increase in augmentation was significantly smaller and practically linear.

The residue weight generally increased with increasing acceleration to a maximum peak (Fig. 3). Beyond this acceleration level the residue weight decreased with increasing acceleration. The point at which this peak occurred appeared to be a strong function of the strand length.

Residue appearance followed a definite pattern of evolution Fig. 4, 5, 6, and 7). At low accelerations the residue took the form of very small spheres. As the acceleration increased, the spheres increased in size. Irregularly shaped pieces then appeared and displayed nodules on their upper surfaces. Further increase in acceleration produced larger irregular pieces with many very small nodules. Finally the residue evolved into a crusty slag flood, spread in intersecting rivers across the surface.

This crusty slag at the highest acceleration levels was virtually hollow on the underneath surface (Fig. 7). It resembled the appearance of a bubbling volcanic process.

The formation of the slag is a function of both burn time and acceleration level. For the quarter-inch strand the slag did not form until 800-1000g, whereas it appeared at 200g for the one-inch strand.

X-Ray powder diffraction data are shown in Table III. For the strand lengths tested, both aluminum and alpha aluminum oxide were identifiable at and below 150g. Also at these low accelerations there were numerous peaks which could not be identified. At and above 200g the aluminum oxide peaks were undetectable; there were also fewer unidentifiable peaks. The aluminum peaks generally continued to increase in intensity as the acceleration was increased.

C. EFFECT OF STRAND LENGTH ON PROPELLANT N6

Strand length appeared to have a significant effect on each of the variables investigated. Augmentation increased with strand length

to a peak and then decreased with increased strand length (Fig. 10). At 500g this peak occurred at or before the shortest length tested, while at 100g the peak augmentation was at a strand length of about 0.75 inches.

It must be noted that the burning rates calculated from the data represent an average value over the entire strand length. They must not be interpreted as instantaneous augmentations at instantaneous strand lengths as the propellant burns.

Residue weight behaved in the same general manner as did augmentation, as the strand length was varied, except the 100g level did not indicate a distinct peak (Fig. 11). The residue appearance followed the same evolution, with increasing strand length, as it did with increasing acceleration (Fig. 4, 5, 6, and 7).

The maximum residue weights occurred at 100g, 200g, and 400g for the two-inch, one-inch, and one-half-inch strand lengths, respectively (Fig. 3). These accelerations are precisely the same values at which the crusty slag first appeared (Fig. 5, 6, and 7).

Residue composition did not appear to be a strong function of propellant strand length. Both aluminum and aluminum oxide were present below 200g. There was no detectable aluminum oxide above 200g, and the aluminum increased in intensity and clarity. This same pattern was true for all strand lengths tested.

In summary, both augmentation and residue weight increased to maximums and then decreased as strand length was increased.

Increasing strand length had the same effect on residue appearance as increasing acceleration. Strand length appeared to have no effect on residue composition.

D. DISCUSSION OF ACCELERATION AND STRAND LENGTH

The augmentation process is generally attributed to the actions of the aluminum particles [Ref. 1 and 3]. This is not the complete mechanism, however, because non-aluminized propellants are also known to augment in a similar manner with increasing acceleration [Ref. 5]. The present discussion is restricted to the effect of the aluminum particles.

At the low accelerations the residue takes the form of distinct spheroids. As the acceleration increases, not only do the spheroids increase in size but the acceleration forces them against the propellant surface causing them to burn in pits. This phenomenon has been observed in quenching studies [Ref. 7]. This pitting of the surface is caused by increased heat transfer through the metallic agglomerates, and increases the effective burning surface area.

At higher accelerations the aluminum appears to flatten over the surface in semi- or full-slag layers. In this condition there is less pitting, but the thermal feedback to the propellant surface is greater than in the zero g condition. Thus at the higher accelerations, the slope of the augmentation curve (Fig. 2, etc.) should decrease, because one of its supporting mechanisms is no longer as effective.

The residue photographs vividly demonstrate the changes occurring in residue form as strand length (burn time) increases. For constant acceleration, the residue was initially in the form of distinct spheroids after one-quarter inch had burned. As the burning progressed farther down the strand the particles accumulated more aluminum, became larger and fewer in number, and did not pit the surface as much. Finally, a slag layer was formed which would cause little increase in surface area due to pitting.

Consequently, if the above augmentation hypothesis is correct, the burning rate would be expected to decrease as strand length is increased. This is precisely what is shown by the burning rate data (Fig. 2). Augmentation still occurs after the slag layer has formed, primarily due to the increased thermal conductivity through the metallic layer.

The residue weight increased with acceleration up to the level at which the slag layer was first observed. Beyond that, residue weight decreased. This is evident in Fig. 3. When the residue is in the form of distinct particles, less of it is consumed in the burning process. After the slag layer is formed, all of the gases from the burning propellant must escape by bubbling through the layer. Evidently this process causes more of the aluminum to be consumed, and hence less residue weight remains.

As strand length increases, more aluminum accumulates on the surface and the flood layer forms at a lower acceleration. Hence, it

would be expected that the peak in post-fire residue weight would occur at lower accelerations as strand length is increased. This also is precisely what the data show in Figure 3.

More striking is the apparent pattern of acceleration and propellant length combinations at which the post-fire residue peaks occurred. The half-inch strand post-fire residue peaked at 400g. Doubling the strand length (and hence the aluminum originally present) reduced the acceleration for peak residue weight, by one-half, to 200g. When the strand length was quadrupled, the acceleration was reduced to one-quarter, i.e., to 100g. This behavior is shown in Figure 8(b).

Because of this strong dependence of the occurrence of maximum residue weight (or surface flooding) on acceleration and burn time (strand length), an attempt was made to normalize the data for propellant N6. Figure 8(a) shows the maximum residue weight, and Fig. 8(b) the acceleration at which it occurred, both as a function of strand length. These two plots clearly indicate the strong dependence of maximum residue weight on acceleration and burn time.

Figure 9 is a normalized plot of residue weight versus acceleration. The residue weight for each strand length is normalized by dividing by the maximum residue weight for that strand length. The acceleration is normalized by dividing by the acceleration at which the maximum residue weight occurred. The normalizing factors were deduced from the curves in Fig. 3. Figure 9 shows the distinct increase to a peak and the subsequent decrease as acceleration

increases. This behavior has been discussed for the individual strand lengths and the plot shows the identical behavior when grouped in the non-dimensional form.

E. EFFECT OF AP SIZE AND BASE BURNING RATE

A comparison of N6 and N7 propellants contrasts both a change in base burning rate and AP size. The average base burning rate of N6 (for half-inch strands and longer) was 0.366 inches per second while for similar strands of N7 it was 0.226 inches per second. AP size of N6 was nine microns and for N7 it was 90 microns. Hence, a comparison of N7 with N6 reflects a decrease in base burning rate and an increase in AP size.

At the lower base burning rate and larger AP size, augmentation increased significantly (Fig. 12) as expected [Ref. 1 and 3]. The augmentation curves for N7 had the same form as those for N6. Residue weight essentially remained the same except for an increase at 100g for the two inch, N7 sample (Fig. 13).

Residue appearance did not change significantly at either strand length or acceleration (Fig. 5, 7, and 14). The same general pattern of residue formation continued to prevail.

At 100g, aluminum and aluminum oxide were present in both of the two inch samples and in the half inch N6 sample. However, only strong aluminum peaks were detected in the half inch N7 sample. At 500g, only aluminum was identified in all samples. In addition, the half inch N7 exhibited very strong unidentifiable peaks.

In summary, decreasing base burning rate and increasing AP size increased augmentation considerably. Residue weight and appearance essentially remained unchanged. Residue composition was generally unchanged except for the shorter strand length. (This indicates that the initial burning phase is possibly different, but that after that they are more similar.)

F. EFFECT OF AP SIZE

N6 and N9 exhibited almost identical average base burning rates: 0.366 inches per second and 0.377 inches per second, respectively. The only significant difference between the two was AP size: nine microns for N6 and 90 microns for N9. In addition, N9 contained one percent of yellow iron oxide as a burning rate catalyst.

In the two-inch strands, AP size had no apparent effect on augmentation (Fig. 15). However, for the one-half inch strands, the larger AP propellant augmented less. The residue weight increased with the larger AP size for the two-inch strand lengths (Fig. 16). The data were insufficient to determine whether the peaks in residue weights occurred at the same accelerations.

The residue samples also exhibited a change in appearance (Fig. 14). The half-inch samples at 100g were essentially the same for N6 and N9 except the N9 spheroids contained small cracks. At 500g, the slag layer had not formed to the extent it had at the smaller AP size. There were still distinct spheroids and irregular pieces that were not of the crusty appearance.

The two-inch N9 samples at both accelerations contained what appeared to be broken, jagged pieces. It was powdery and tended to crumble easily. Because of this tendency some significant portion of the crumbled appearance could have been induced when the inhibitor case walls were removed. When these samples were prepared for the X-Ray diffraction it was noted that they crushed extremely easily.

X-Ray powder diffraction revealed that the half-inch N9 samples contained aluminum and aluminum oxide at low acceleration, and primarily aluminum at high acceleration, in the same manner as the N6 samples. However, the powdery two-inch samples were completely unidentifiable. Neither aluminum, aluminum oxide, iron oxide (Fe_2O_3), iron oxide (Fe_3O_4), or iron could be identified at either acceleration. Iron atoms were known to be present in some form, however, because of the fluorescence which was obtained from the residue. This residue analysis was certainly consistent with the residue appearance; it was physically different and it was chemically different from that for propellant N6.

G. EFFECT OF BASE BURNING RATE

N7 exhibited an average base burning rate of 0.226 inches per second while N9 was 0.377; otherwise the two propellants were identical except for the catalyst agent. The lower base burning rate N7 augmented significantly more than the N9 (Fig. 17). The N7 augmentation was generally 30 - 40% higher while its base burning rate was 40% lower.

Residue weight was not a function of base burning rate for the half-inch strands. The two-inch N7 produced more residue at 100g than N9. At 500g, there was a wide spread in the two-inch N9 residue weight, which made any comparison difficult (Fig. 18).

The N7 residue appearances were the same as the N6 samples, therefore the comparisons of N6 and N9 in residue appearance are also valid here. Powder diffraction analysis identified the same residue components in N7 as N6, except aluminum oxide was missing in the half-inch sample of N7 at 100g. Consequently the residue analysis comparison between N6 and N9 is generally valid between N7 and N9.

H. DISCUSSION OF EFFECT OF AP SIZE AND BASE BURNING RATE

The data plotted in Fig. 17 indicate a significant increase in burning rate augmentation for the lower base burning rates. At the slower burning rates there would be a lower gas velocity leaving the burning propellant surface. This would cause a lower drag or pressure force on the particles at a given acceleration, resulting in a greater imbalance of forces which would hold the particles more strongly against the surface. This action would result in increased heat transfer and pitting. Hence, this increase in augmentation at the lower burning rate would be expected. The tabulated data (Table II) show that although the N7 experienced greater augmentation, its burning rate never reached that of the N9 at any acceleration level tested.

The greater pressure force on the metallic particles in the propellant with the higher base burning rate could be expected to blow many

of the particles completely away from the combustion region. If this were true, a lower residue weight would be expected for the N9 samples. This did not occur except for the 100g two-inch samples.

Evidently the metallic particles are not removed completely. They remain at an increased distance from the surface, which reduces the thermal feedback to the surface and hence decreases burning rate augmentation.

It would be expected that an increase in AP size would have a significant effect on the pitting characteristics of the burning propellant. The lack of change in augmentation of the N9 two-inch sample from the N6 sample was anticipated. The two-inch residues were in the form of flood layers, a form where the pitted characteristic of the surface is not as significant.

A greater effect on augmentation would be expected for the half-inch samples where the residue was in the form of spheroids. The half-inch N9 samples did not augment as much as the half-inch N6 samples. This indicates that an increase in AP size either reduced the heat transfer to the surface or reduced the effective burning surface area.

In the half-inch samples the final residue appearance did not change appreciably. N9 did exhibit somewhat more particles which were slightly smaller in size. This could be expected since the larger AP particles in N9 would not permit the aluminum agglomerates to coalesce as readily as the more homogeneous surface of the propellant with the smaller AP size (N6). In both cases, the particles were of the

same chemical composition. Consequently, there does not appear to be a concise, well-defined explanation for the augmentation decrease with the larger AP size for the half-inch strands.

No explanation can be offered for the behavior of the two-inch N9 samples. However, it does interject a strong note of caution. It is quite possible that the iron oxide catalyst does not merely increase the rate of the reaction but also changes the chemical process altogether. This could be expected primarily in the longer lengths due to the increased time for the accumulation of the iron oxide on the surface. The two-inch samples did exhibit a much stronger fluorescence than the half-inch samples during X-Ray diffraction. The one percent iron-oxide concentration in the propellant caused no fluorescence whatsoever when exposed to the X-Rays.

I. APPLICABILITY OF THE CROWE, et al., MODEL

The Crowe, et al., model is derived and presented in Ref. 3. It is therein simplified (valid for augmentation ratios in excess of 1.2) to:

$$\frac{\dot{r}}{\dot{r}_o} = 2\left[\frac{r_s}{a}\left(\frac{\rho_p P_c \alpha}{r_s}\right)^{1/4} \frac{K'}{\rho_s \dot{r}_o (1-w)} - .2\right] + 1$$

where

r_s = radius of equivalent sphere of same particle mass

a = major radius of oblate spheroid

ρ_p = particle density

P_c = combustion pressure

α = acceleration

K' = a constant for each propellant formulation

ρ_s = propellant surface density

$\dot{r}_o$ = base burning rate

w = percentage of metal in propellant

The model is based on the hypothesis that the augmented burning rate is the result of increased heat transfer to the propellant surface from a hot particle buoyed above the surface by evolving gases.

For a given propellant at constant pressure, the model further reduces to:

$$\frac{\dot{r}}{\dot{r}_o} = 2\left[\frac{r_s}{a}\left(\frac{\rho_p \alpha}{r_s}\right)^{1/4} K'' - .2\right] + 1$$

K'' includes those parameters dependent only on pressure and propellant formulation. The model includes an explicit dependence of augmentation on acceleration. However, particle oblateness (r_s/a), particle density (ρ_p), and particle size (r_s) are themselves dependent on the acceleration level and/or burn time.

The model does not include an explicit dependence on burn time (strand length). The data in this investigation did not show a variation of particle density (residue composition) as a function of burn time. Residue composition appeared to vary only with acceleration. Consequently the effect of burn time on augmentation must be evidenced through particle oblateness and size if the model is to be valid.

Since particle density is not a function of time, for a given propellant at constant acceleration and pressure the model takes the form:

$$\frac{\dot{r}}{\dot{r}_o} = 2\left[\frac{r_s}{a}\left(\frac{1}{r_s}\right)^{1/4} K''' - .2\right] + 1$$

Previous investigations and the data herein show a decreasing augmentation with increasing burn time (Fig. 2). If the model is to correctly predict this trend, the product $(r_s/a)(1/r_s)^{\frac{1}{4}}$ must decrease with burn time. The residue photographs (Fig. 4, 5, 6, and 7) show that the particles become more oblate (r_s/a decreases) as burn time increases at a constant acceleration. Additionally, the particle size increases markedly, hence $(1/r_s)^{\frac{1}{4}}$ also decreases. Consequently their product does indeed decrease with burn time and the model does predict the correct trend.

The Crowe, et al., model for the flooded state becomes [Ref. 3]:

$$\frac{\dot{r}}{\dot{r}_o} = 2\left[\frac{K''''}{(W_r)^{1/4}} - .2\right] + 1$$

where W_r is the residue weight. The model thus predicts that after the surface floods, augmentation is a function of residue weight only. The data from this investigation show that after flooding, augmentation continues to increase at a low rate. The data also show that the level of acceleration at which the surface flooded generally coincided with the point of maximum residue weight. Hence higher acceleration levels after flooding decrease residue weight. Thus, the model correctly indicates the observed increase in augmentation with increasing acceleration in the flooded state.

To apply the Crowe et al., model, the functional dependence of residue oblateness and size on burn time must be known. Figures 19 and 20 show the relation between total post-fire residue weight and burn time for 100g and 500g respectively.

In both of these logarithmic plots the more numerous data points for the N6 propellants are essentially linear. This linear variation indicated a functional relationship of the form:

$$W = at^n$$

where

W = residue weight

t = burn time

n = slope of the log plot

a = constant dependent on propellant, acceleration, and pressure

The exponent, n, was graphically determined to be 1.82 at 100g and 0.425 at 500g.

If the data for N7 and N9 are also assumed to vary linearly in the logarithmic plot(the data were insufficient to confirm this variation), it is noted that the slopes were essentially the same as the N6 curve. Hence the functional dependence of residue weight on burn time for a given acceleration is very weak, as AP size and base burning rate are varied.

V. CONCLUSIONS

Augmentation of propellant burning rates increases with increasing acceleration. At low accelerations, the post-fire residue is initially in the form of distinct spheroids. As acceleration increases, the form changes to larger discs, large irregular pieces, and eventually to a partial or full crusty slag layer. The residue form changes in a similar manner with increasing burn time. However, the number of distinct residue particles decreases rapidly as burn time increases. When the residue is in the form of distinct spheroids, the burning rate augmentation is more sensitive to acceleration.

Residue composition appears to be a strong function of acceleration and does not change significantly with burn time. At low accelerations, the residue contains both aluminum and aluminum oxide; the aluminum oxide was not detectable at high accelerations.

As acceleration increases, residue weight increases to a peak and then decreases. The maximum residue weight occurs at the same acceleration where the surface initially floods. This acceleration level decreases as strand length increases.

Average burning rate augmentation decreases with increasing burn time while the residue weight increases.

Decreasing base burning rate significantly increases the burning rate augmentation. Base burning rate had little effect on residue weight, appearance, and composition.

Iron Oxide (Fe_2O_3) catalyst apparently changes the metallic combustion process when it is present in sufficient quantities.

The Crowe, et al., model predicts the correct augmentation trend as a function of burn time if the time-history of the metallic agglomerates is known. The precise functional dependence of burning rate augmentation on burn time remains to be determined. The model predicts the correct augmentation trend after the burning surface becomes flooded.

At a given acceleration, AP size and base burning rate have little effect on the functional dependence of residue weight on burn time for propellants with fixed aluminum content and size.

TABLE I. PROPELLANT DESIGNATIONS AND FORMULATIONS

Prop. Desig.	Weight % AP	AP Size (μ)	Weight % PBAN	Weight % Al	Al Size (μ)	Weight % Fe_2O_3
N6	67.00	9	18.00	15.00	44	---
N7	67.00	90	18.00	15.00	44	---
N9	66.33	90	17.82	14.85	44	1.00

TABLE II. PROPELLANT BURNING RATE AND RESIDUE WEIGHT DATA

PROPELLANT SAMPLE	LENGTH (INCHES)	ACCELERATION (g's)	BURNING RATE (ips)	AUGMENTATION ($\dot{r}/\dot{r}_o$)	RESIDUE WEIGHT (mg)	RESIDUE WEIGHT (mg/cc)	PRESSURE (psia)
N6-1Q	0.255	0	0.385	1.00	0.0	0.0	508
N6-2Q	0.245	0	0.373	1.00	0.0	0.0	511
N6-3Q	0.242	99	0.423	1.12	6.1	6.3	502
N6-8Q	0.248	149	0.468	1.24	29.3	29.3	501
N6-10Q	0.250	150	0.472	1.25	23.3	22.7	534
N6-4Q	0.240	200	0.500	1.32	24.8	25.6	501
N6-9Q	0.245	251	0.498	1.31	22.7	23.0	499
N6-5Q	0.242	350	0.523	1.38	39.3	40.3	505
N6-6Q	0.247	500	0.558	1.47	50.6	50.8	507
N6-7Q	0.241	1004	0.545	1.44	57.6	59.3	505
N6-1H	0.503	0	0.374	1.00	0.0	0.0	504
N6-5H	0.500	0	0.357	1.00	0.0	0.0	508
N6-2H	0.500	50	0.395	1.08	10.3	5.1	493

TABLE II. PROPELLANT BURNING RATE AND RESIDUE WEIGHT DATA (CONT.)

PROPELLANT SAMPLE	LENGTH (INCHES)	ACCELERATION (g's)	BURNING RATE (ips)	AUGMENTATION ($\dot{r}/\dot{r}_o$)	RESIDUE WEIGHT (mg)	RESIDUE WEIGHT (mg/cc)	PRESSURE (psia)
N6-6H	0.503	99	0.434	1.19	47.7	23.5	508
N6-10H	0.494	151	0.437	1.20	70.1	35.2	517
N6-7H	0.500	201	0.483	1.32	36.5	18.1	518
N6-13H	0.518	200	0.471	1.29	43.8	20.6	535
N6-4H	0.501	345	0.466	1.28	53.6	26.5	494
N6-8H	0.498	350	---	---	99.6	49.6	---
N6-11H	0.510	496	0.477	1.30	69.8	33.9	514
N6-9H	0.495	994	0.505	1.38	50.6	25.3	518
N6-1I	0.996	0	0.369	1.00	0.0	0.0	514
N6-8I	0.955	0	0.358	1.00	0.0	0.0	516
N6-10I	0.980	0	0.370	1.00	0.0	0.0	515
N6-9I	0.989	50	---	---	42.2	10.6	---
N6-2I	1.030	98	0.427	1.18	112.6	27.1	513

TABLE II. PROPELLANT BURNING RATE AND RESIDUE WEIGHT DATA (CONT.)

PROPELLANT SAMPLE	LENGTH (INCHES)	ACCELERATION (g's)	BURNING RATE (ips)	AUGMENTATION ($\dot{r}/\dot{r}_o$)	RESIDUE WEIGHT (mg)	RESIDUE WEIGHT (mg/cc)	PRESSURE (psia)
N6-14I	1.018	100	0.435	1.19	119.7	28.7	539
N6-6I	0.996	150	0.430	1.18	101.6	25.3	514
N6-3I	1.047	200	0.464	1.28	86.6	20.5	514
N6-4I	0.983	349	0.451	1.24	103.1	26.0	512
N6-12I	1.014	349	0.453	1.24	112.4	27.5	503
N6-7I	0.989	501	0.471	1.30	100.9	25.3	513
N6-5I	1.016	1001	0.493	1.36	59.1	14.4	505
N6-33T	2.041	0	0.372	1.00	0.0	0.0	531
N6-34T	2.045	0	0.361	1.00	0.0	0.0	508
N6-29T	2.027	101	0.407	1.11	275.8	33.7	524
N6-30T	2.028	100	0.421	1.15	293.6	35.7	529
N6-36T	2.037	504	0.446	1.22	117.2	14.3	525
N6-32T	2.016	501	0.444	1.21	154.8	19.0	520

TABLE II. PROPELLANT BURNING RATE AND RESIDUE WEIGHT DATA (CONT.)

PROPELLANT SAMPLE	LENGTH (INCHES)	ACCELERATION (g's)	BURNING RATE (ips)	AUGMENTATION ($\dot{r}/\dot{r}_o$)	RESIDUE WEIGHT (mg)	RESIDUE WEIGHT (mg/cc)	PRESSURE (psia)
N7-5H	0.525	0	0.220	1.00	0.0	0.0	505
N7-6H	0.525	0	0.225	1.00	0.0	0.0	504
N7-1H	0.525	100	0.351	1.58	46.7	22.1	502
N7-2H	0.525	100	0.337	1.51	56.9	26.9	504
N7-7H	0.531	100	0.340	1.53	---	---	508
N7-4H	0.525	493	0.388	1.74	68.4	32.3	504
N7-3H	0.525	---	---	---	74.8	35.3	---
N7-1T	2.005	0	0.230	1.00	0.0	0.0	518
N7-7T	2.000	0	0.228	1.00	0.0	0.0	514
N7-1T	2.002	101	0.289	1.26	460.7	57.1	530
N7-3T	2.005	501	0.363	1.58	139.3	17.2	526
N7-4T	2.000	504	0.358	1.56	137.8	17.1	526
N9-6H	0.521	0	0.378	1.00	0.0	0.0	515

TABLE II. PROPELLANT BURNING RATE AND RESIDUE WEIGHT DATA (CONT.)

PROPELLANT SAMPLE	LENGTH (INCHES)	ACCELERATION (g's)	BURNING RATE (ips)	AUGMENTATION ($\dot{r}/\dot{r}_o$)	RESIDUE WEIGHT (mg)	RESIDUE WEIGHT (mg/cc)	PRESSURE (psia)
N9-9H	0.518	0	0.382	1.00	0.0	0.0	545
N9-1H	0.525	98	0.430	1.14	53.4	25.2	559
N9-2H	0.525	98	0.415	1.10	46.0	21.7	503
N9-3H	0.525	488	0.441	1.17	93.3	44.1	494
N9-4H	0.531	491	0.474	1.26	81.7	38.2	495
N9-42T	2.025	0	0.376	1.00	0.0	0.0	545
N9-43T	2.011	100	0.410	1.09	353.9	43.6	519
N9-46T	2.020	100	---	---	359.0	44.1	---
N9-50T	2.030	501	0.458	1.22	325.8	39.8	522
N9-48T	2.030	501	0.429	1.14	116.0	14.2	513

TABLE III. X-RAY POWDER DIFFRACTION DATA

N6-6H (half inch, 100g)

TWO-THETA	INTENSITY	IDENTIFICATION	TWO-THETA	INTENSITY	IDENTIFICATION
31.7	36		57.65	32	Al_2O_3
32.25	26		60.0	38	
32.6	26		60.2	24	
34.8	48		61.0	20	
35.3	114	Al_2O_3	61.3	20	
36.5	32		61.6	32	
36.8	32		66.1	20	
38.7	56	Al	66.3	20	
39.1	28		66.6	72	Al_2O_3
43.2	34		67.25	112	
43.6	34	Al_2O_3	68.3	34	
44.85	28	Al	68.45	34	Al_2O_3
45.0	26		77.2	20	
45.25	44		78.35	22	Al
52.7	26	Al_2O_3			

N6-10H, half inch, 150g

TWO-THETA	INTENSITY	IDENTIFICATION	TWO-THETA	INTENSITY	IDENTIFICATION
32.1	31		38.6	54	Al
32.6	30		41.2	26	
34.8	30	Al (β)	43.2	19	
35.3	36	Al_2O_3	43.5	15	Al_2O_3
36.7	26		44.8	19	Al

TABLE III. X-RAY POWDER DIFFRACTION DATA (CONT.)

N6-10H, half inch, 150g (Cont.)

TWO-THETA	INTENSITY	IDENTIFICATION	TWO-THETA	INTENSITY	IDENTIFICATION
45.8	72		60.0	29	
46.3	32		61.6	18	
51.7	10		65.3	10	Al
52.6	10	Al_2O_3	66.8	64	
55.2	10		67.2	88	
58.2	28		78.4	25	Al
59.5	16				

N6-7H, half inch, 200g

TWO-THETA	INTENSITY	IDENTIFICATION	TWO-THETA	INTENSITY	IDENTIFICATION
32.0	30		46.6	30	
32.3	32		58.2	30	Al (β)
34.7	70	Al (β)	60.8	25	
38.5	330	Al	65.3	47	Al
40.3	22	Al (β)	66.9	40	
44.8	70	Al	78.4	45	Al
45.8	97				

N6-4H, half inch, 350g

TWO-THETA	INTENSITY	IDENTIFICATION	TWO-THETA	INTENSITY	IDENTIFICATION
32.0	32		34.7	42	Al (β)
32.6	27		38.4	265	Al

TABLE III. X-RAY POWDER DIFFRACTION DATA (CONT.)

N6-4H, half inch, 350g (Cont.)

TWO-THETA	INTENSITY	IDENTIFICATION	TWO-THETA	INTENSITY	IDENTIFICATION
40.4	70	Al (β)	65.2	125	Al
43.7	47		69.7	35	Al (β)
44.8	147	Al	73.0	25	Al (β)
55.2	50		78.4	115	Al
58.2	47	Al (β)	82.6	27	Al

N6-11H, half inch, 500g

TWO-THETA	INTENSITY	IDENTIFICATION	TWO-THETA	INTENSITY	IDENTIFICATION
32.0	30		48.3	20	
32.5	32		55.2	32	
34.7	42	Al (β)	58.2	32	Al (β)
36.1	22		65.3	90	Al
38.5	190	Al	69.7	22	Al (β)
40.3	45	Al (β)	73.1	25	Al (β)
43.7	40		78.2	80	Al
44.8	107	Al			

N6-9H, half inch, 1000g

TWO-THETA	INTENSITY	IDENTIFICATION	TWO-THETA	INTENSITY	IDENTIFICATION
31.4	27		34.8	42	Al (β)
32.0	32		36.3	35	
32.7	17		38.5	212	Al

TABLE III. X-RAY POWDER DIFFRACTION DATA (CONT.)

N6-9H, half inch, 1000g (Cont.)

TWO-THETA	INTENSITY	IDENTIFICATION	TWO-THETA	INTENSITY	IDENTIFICATION
40.4	55	Al (β)	65.3	82	Al
43.8	25		69.7	20	Al (β)
44.9	117	Al	73.1	32	Al (β)
48.5	17		78.4	72	Al
55.3	45		82.6	20	Al
58.3	30	Al (β)			

N6-2I, one inch, 100g

TWO-THETA	INTENSITY	IDENTIFICATION	TWO-THETA	INTENSITY	IDENTIFICATION
25.4	65		52.6	34	Al_2O_3
29.0	19		57.6	65	Al_2O_3
29.5	14		58.2	47	
32.3	48		65.2	23	Al
32.6	64		66.6	52	Al_2O_3
35.2	84	Al_2O_3	66.9	46	
38.6	68	Al	67.2	42	
43.5	39	Al_2O_3	68.3	41	Al_2O_3
44.7	32	Al	69.8	20	
45.7	46		78.3	24	Al

TABLE III. X-RAY POWDER DIFFRACTION DATA (CONT.)

N6-6I, one inch, 150g

TWO-THETA	INTENSITY	IDENTIFICATION	TWO-THETA	INTENSITY	IDENTIFICATION
32.2	34		44.8	81	Al
32.6	46		48.8	17	
34.7	35	Al (β)	52.6	19	Al_2O_3
35.3	30	Al_2O_3	58.2	46	Al (β)
37.3	24		65.2	50	Al
38.3	89		66.6	27	Al_2O_3
38.6	136	Al	67.1	28	
40.3	19	Al (β)	68.3	24	Al_2O_3
41.2	22		69.8	22	Al (β)
43.5	21	Al_2O_3	78.4	56	Al

N6-3I, one inch, 200g

TWO-THETA	INTENSITY	IDENTIFICATION	TWO-THETA	INTENSITY	IDENTIFICATION
32.2	40		48.7	16	
32.7	48		55.2	19	
34.7	41	Al (β)	57.7	16	
38.5	153	Al	58.2	35	Al (β)
40.4	32	Al (β)	65.2	55	Al
43.8	27		78.4	50	Al
44.8	68	Al			

TABLE III. X-RAY POWDER DIFFRACTION DATA (CONT.)

N6-4I, one inch, 350g

TWO-THETA	INTENSITY	IDENTIFICATION	TWO-THETA	INTENSITY	IDENTIFICATION
32.3	27		55.2	19	
34.7	44	Al (β)	58.1	28	Al (β)
38.5	156	Al	65.2	52	Al
40.3	29	Al (β)	69.6	22	Al (β)
43.7	23		72.7	14	
44.7	83	Al	75.2	20	
48.4	18		78.3	48	Al

N6-7I, one inch, 500g

TWO-THETA	INTENSITY	IDENTIFICATION	TWO-THETA	INTENSITY	IDENTIFICATION
32.0	22		55.2	26	
32.7	19		58.2	38	Al (β)
34.8	24	Al (β)	65.3	58	Al
38.5	117	Al	69.8	22	Al (β)
40.3	26	Al (β)	78.5	62	Al
43.6	19		82.5	25	Al
44.8	88	Al			

N6-5I, one inch, 1000g

TWO-THETA	INTENSITY	IDENTIFICATION	TWO-THETA	INTENSITY	IDENTIFICATION
31.8	19		32.6	23	
32.1	22		34.7	35	Al (β)

TABLE III. X-RAY POWDER DIFFRACTION DATA (CONT.)

N6-5I, one inch, 1000g (Cont.)

TWO-THETA	INTENSITY	IDENTIFICATION	TWO-THETA	INTENSITY	IDENTIFICATION
36.1	23		44.4	44	
36.4	27		44.6	70	
37.3	21		44.8	86	Al
38.3	106		58.2	27	Al (β)
38.6	142	Al	60.8	23	
39.4	23		61.5	21	
40.3	37	Al (β)	65.2	59	Al
42.0	20		70.3	19	
43.9	36		78.4	52	Al

N6-30T, two inch, 100g

TWO-THETA	INTENSITY	IDENTIFICATION	TWO-THETA	INTENSITY	IDENTIFICATION
25.6	32		41.2	18	
29.2	20		43.5	64	Al_2O_3
32.2	80		44.8	40	Al
32.6	90	Al_2O_3	45.7	44	
34.9	72		48.75	18	
35.25	80		52.65	24	Al_2O_3
37.3	40		57.65	50	Al_2O_3
38.45	94	Al	58.15	56	
39.9	22		59.85	18	
40.4	21		61.45	19	

TABLE III. X-RAY POWDER DIFFRACTION DATA (CONT.)

N6-30T, two inch, 100g (Cont.)

TWO-THETA	INTEN-SITY	IDENTIFI-CATION	TWO-THETA	INTEN-SITY	IDENTIFI-CATION
65.25	36	Al	68.35	38	Al_2O_3
66.75	50	Al_2O_3	69.9	20	
67.15	52		78.45	26	Al

N6-36T, two inch, 500g

TWO-THETA	INTEN-SITY	IDENTIFI-CATION	TWO-THETA	INTEN-SITY	IDENTIFI-CATION
32.1	50		44.8	105	Al
32.6	55		55.3	65	
34.7	40	Al (β)	58.25	50	Al (α)
36.2	40		61.45	30	
38.5	115	Al	65.25	70	Al
40.35	85	Al (β)	73.0	67	
43.8	55		78.45	52	Al

N7-1/2H, half inch, 100g

TWO-THETA	INTEN-SITY	IDENTIFI-CATION	TWO-THETA	INTEN-SITY	IDENTIFI-CATION
32.6	40		55.35	27	
34.8	65	Al (β)	58.3	37	Al (β)
38.6	230	Al	65.35	95	Al
40.4	50	Al (β)	67.05	40	
44.9	130	Al	69.7	30	Al (β)
45.85	25		78.5	100	Al

TABLE III. X-RAY POWDER DIFFRACTION DATA (CONT.)

N7-3/4H, half inch, 500g

TWO-THETA	INTENSITY	IDENTIFICATION	TWO-THETA	INTENSITY	IDENTIFICATION
32.6	35		55.4	60	
34.75	60	Al (β)	58.35	40	Al (β)
36.2	45		61.55	27	
38.6	280	Al	65.35	115	Al
40.4	80	Al (β)	69.75	35	Al (β)
43.85	60		73.15	45	
44.9	160	Al	78.5	90	Al
48.6	20		82.7	30	

N7-2T, two inch, 100g

TWO-THETA	INTENSITY	IDENTIFICATION	TWO-THETA	INTENSITY	IDENTIFICATION
32.6	210		52.7	40	Al_2O_3
35.25	95	Al_2O_3	55.3	32	
38.55	80	Al	57.9	80	Al_2O_3
40.2	30		61.4	30	
43.45	95	Al_2O_3	65.2	37	Al
44.8	50	Al	66.8	55	Al_2O_3
45.85	30		68.35	55	Al_2O_3
48.85	28		78.45	22	Al

TABLE III. X-RAY POWDER DIFFRACTION DATA (CONT.)

N7-4T, two inch, 500g

TWO-THETA	INTENSITY	IDENTIFICATION	TWO-THETA	INTENSITY	IDENTIFICATION
32.55	60		55.2	55	
34.65	40	Al (β)	58.2	50	Al (β)
38.45	150	Al	65.2	65	Al
40.25	70	Al (β)	73.0	35	Al (β)
43.7	55		78.4	55	Al
44.75	100	Al			

N9-1/2H, half inch, 100g

TWO-THETA	INTENSITY	IDENTIFICATION	TWO-THETA	INTENSITY	IDENTIFICATION
31.6	27		52.5	28	Al_2O_3
32.2	23		52.9	38	
35.05	49		57.6	38	
35.45	42	Al_2O_3	59.45	18	
36.7	28		60.0	22	
38.7	66	Al	61.0	22	
41.1	24		61.45	22	
43.15	40		65.3	28	Al
43.45	48	Al_2O_3	66.75	60	Al_2O_3
44.95	38	Al	67.3	58	
45.7	90		68.45	46	Al_2O_3
46.45	40		77.35	18	
47.5	14		78.45	22	Al

TABLE III. X-RAY POWDER DIFFRACTION DATA (CONT.)

N9-3/4H, half inch, 500g

TWO-THETA	INTENSITY	IDENTIFICATION	TWO-THETA	INTENSITY	IDENTIFICATION
32.4	22		44.6	60	Al
34.7	26	Al (β)	55.25	19	
36.1	26		58.35	14	Al (β)
38.55	53	Al	65.1	27	Al
40.25	32	Al (β)	73.2	20	Al (β)
43.35	46		78.4	28	Al
43.8	37				

N9-46T, two inch, 100g

TWO-THETA	INTENSITY	IDENTIFICATION	TWO-THETA	INTENSITY	IDENTIFICATION
32.3	30		45.75	42	
32.7	38		48.9	12	
35.4	38		57.7	26	
36.8	16		58.15	24	
37.7	22		59.8	16	
38.5	22		64.7	14	
39.15	21		66.75	52	
40.2	24		67.1	50	
43.35	68		69.9	14	
44.6	54				

TABLE III. X-RAY POWDER DIFFRACTION DATA (CONT.)

N9-48T, two inch, 500g

TWO-THETA	INTENSITY	IDENTIFICATION	TWO-THETA	INTENSITY	IDENTIFICATION
32.7	26		45.9	20	
39.4	28		58.4	14	
42.95	48		66.9	24	
43.9	92				

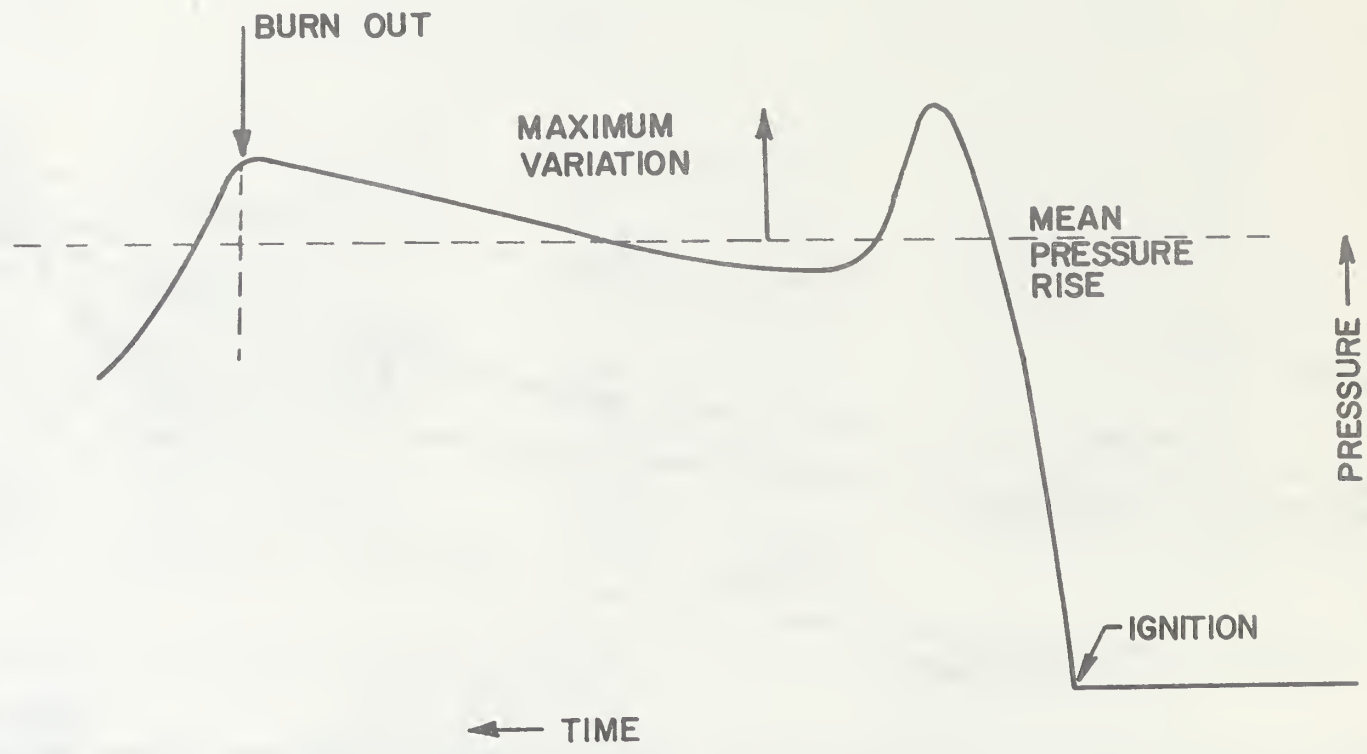

FIGURE I. TYPICAL PRESSURE – TIME TRACE

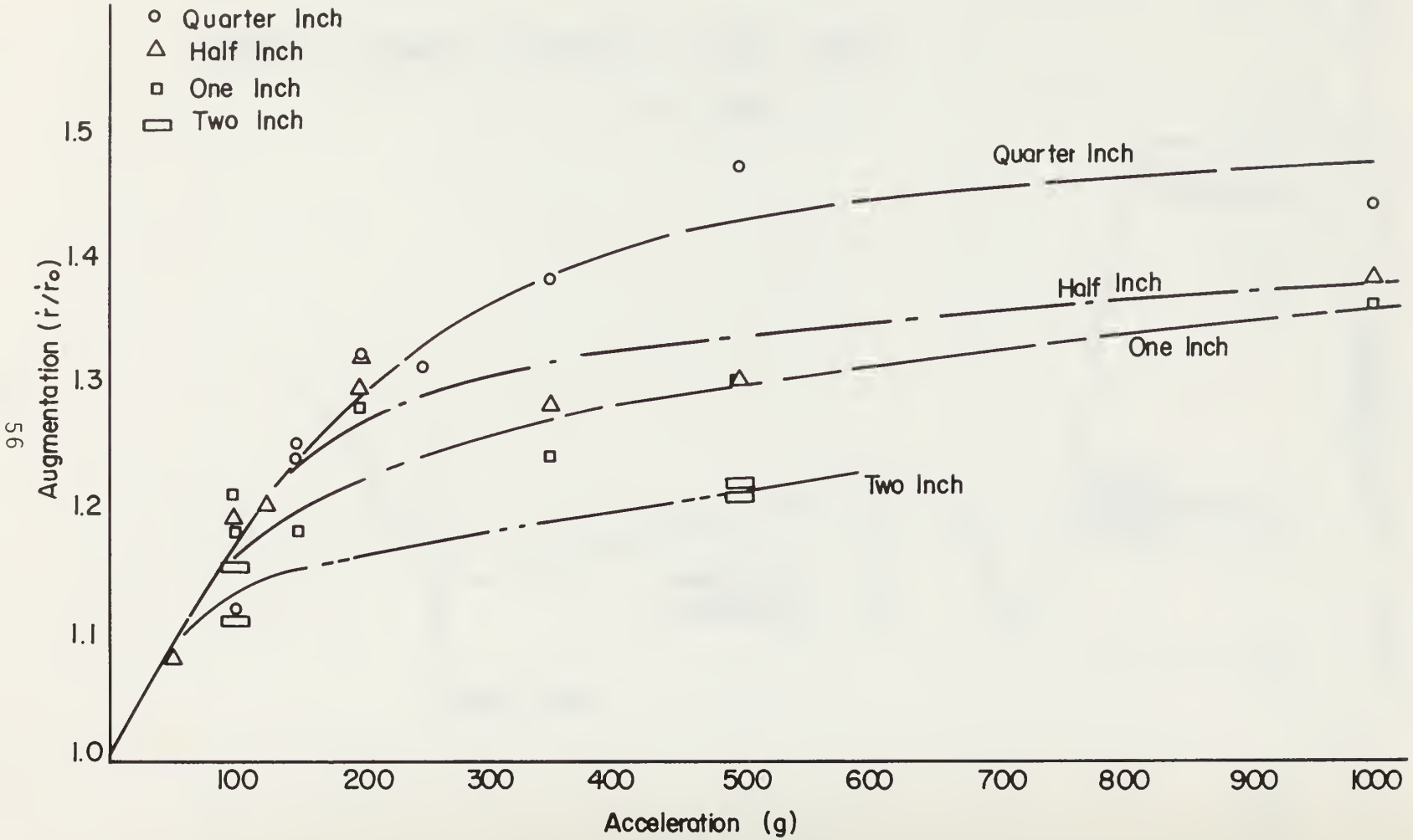

FIGURE 2. EFFECT OF ACCELERATION ON AUGMENTATION

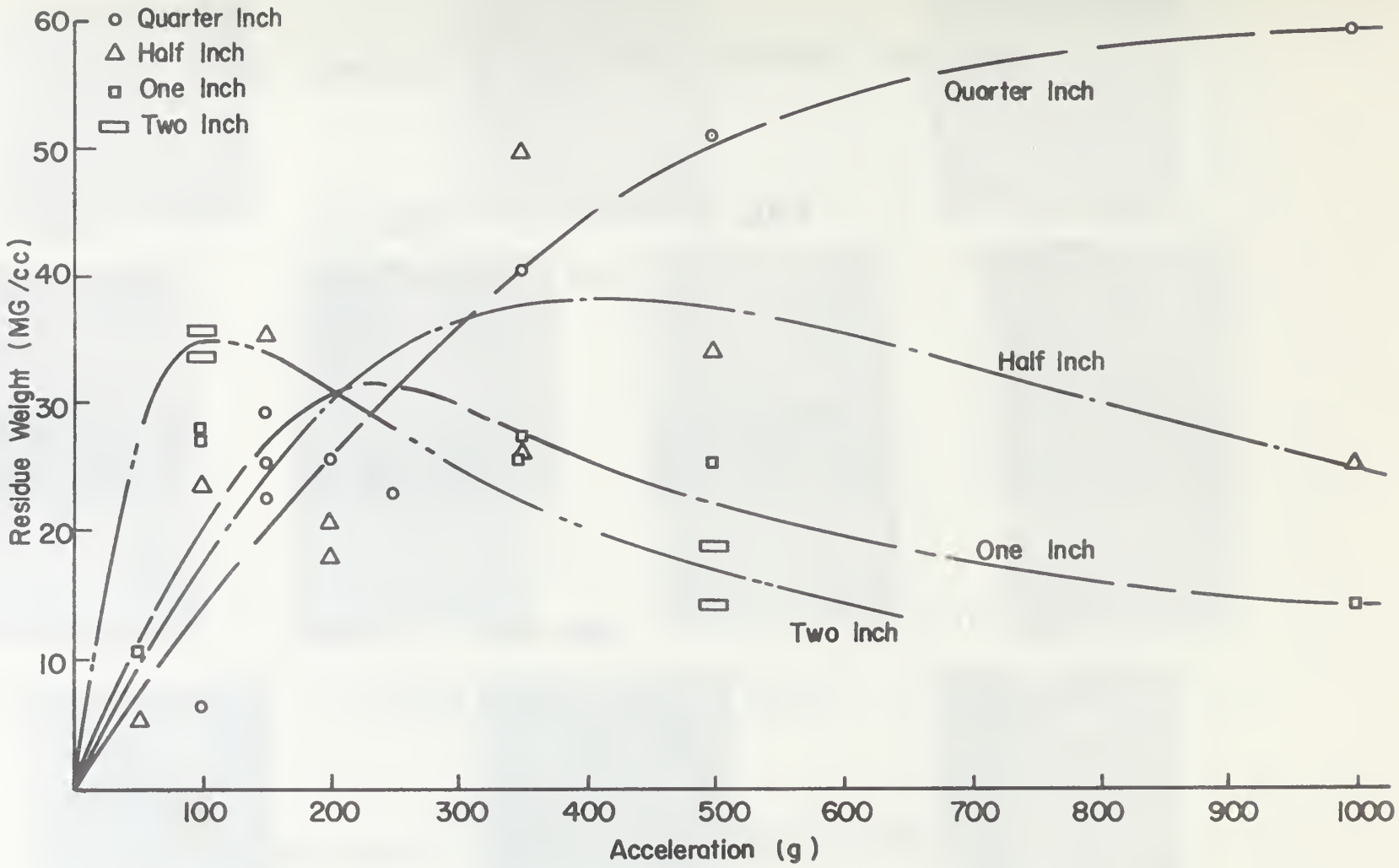

FIGURE 3. EFFECT OF ACCELERATION ON RESIDUE WEIGHT

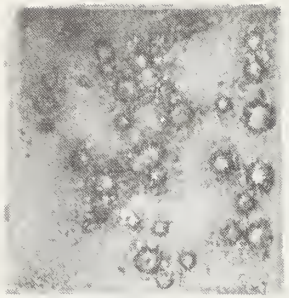

(a) 100g

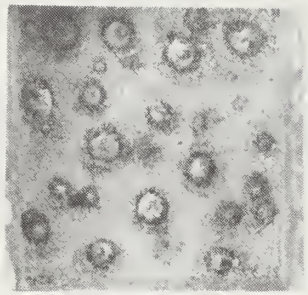

(b) 150g

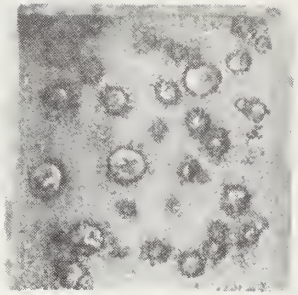

(c) 200g

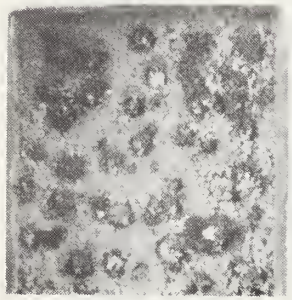

(d) 250g

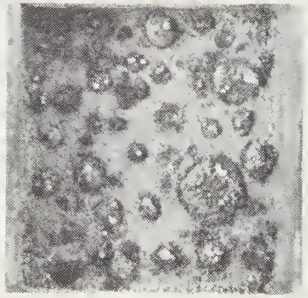

(e) 350g

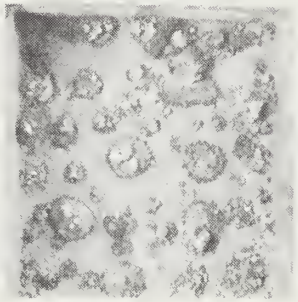

(f) 500g

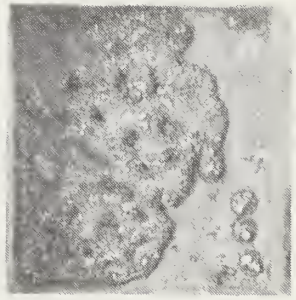

(g) 1000g

FIGURE 4. N6 QUARTER INCH STRAND RESIDUE (MAG. 3X)

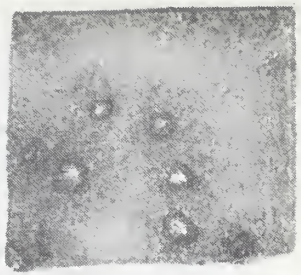

(a) 50g

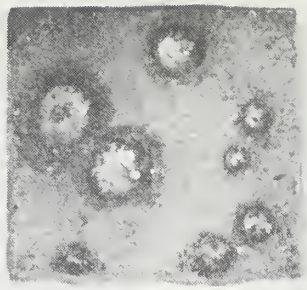

(b) 100g

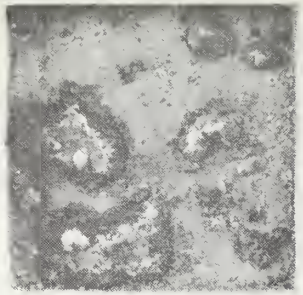

(c) 150g

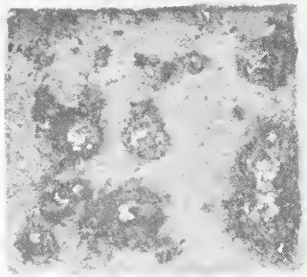

(d) 200g

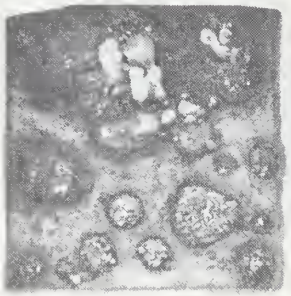

(e) 350g

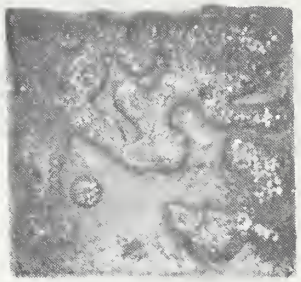

(f) 500g

(g) 1000g

FIGURE 5. N6 HALF INCH STRAND RESIDUE (MAG. 3X)

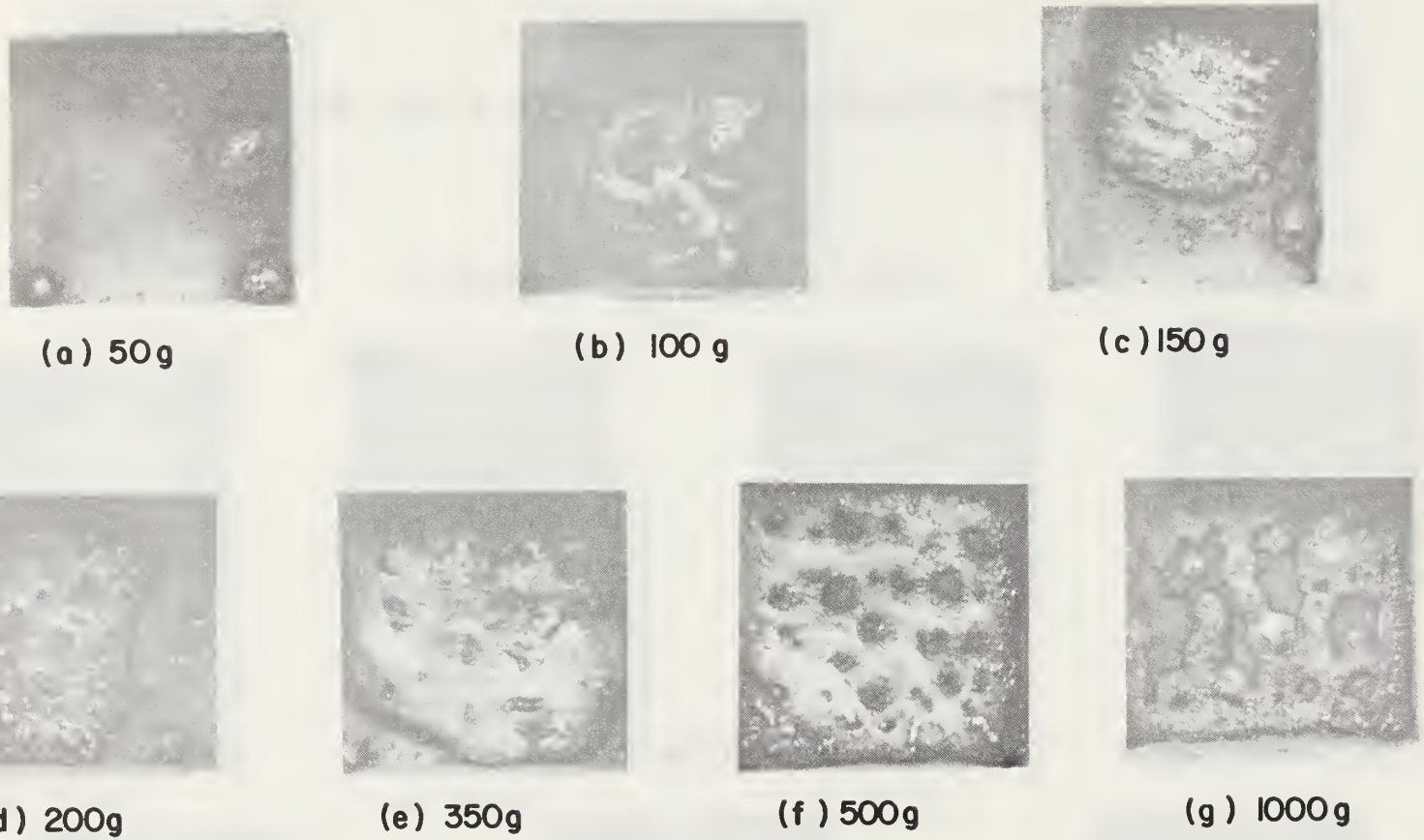

FIGURE 6. N6 ONE INCH STRAND RESIDUE (MAG-3X)

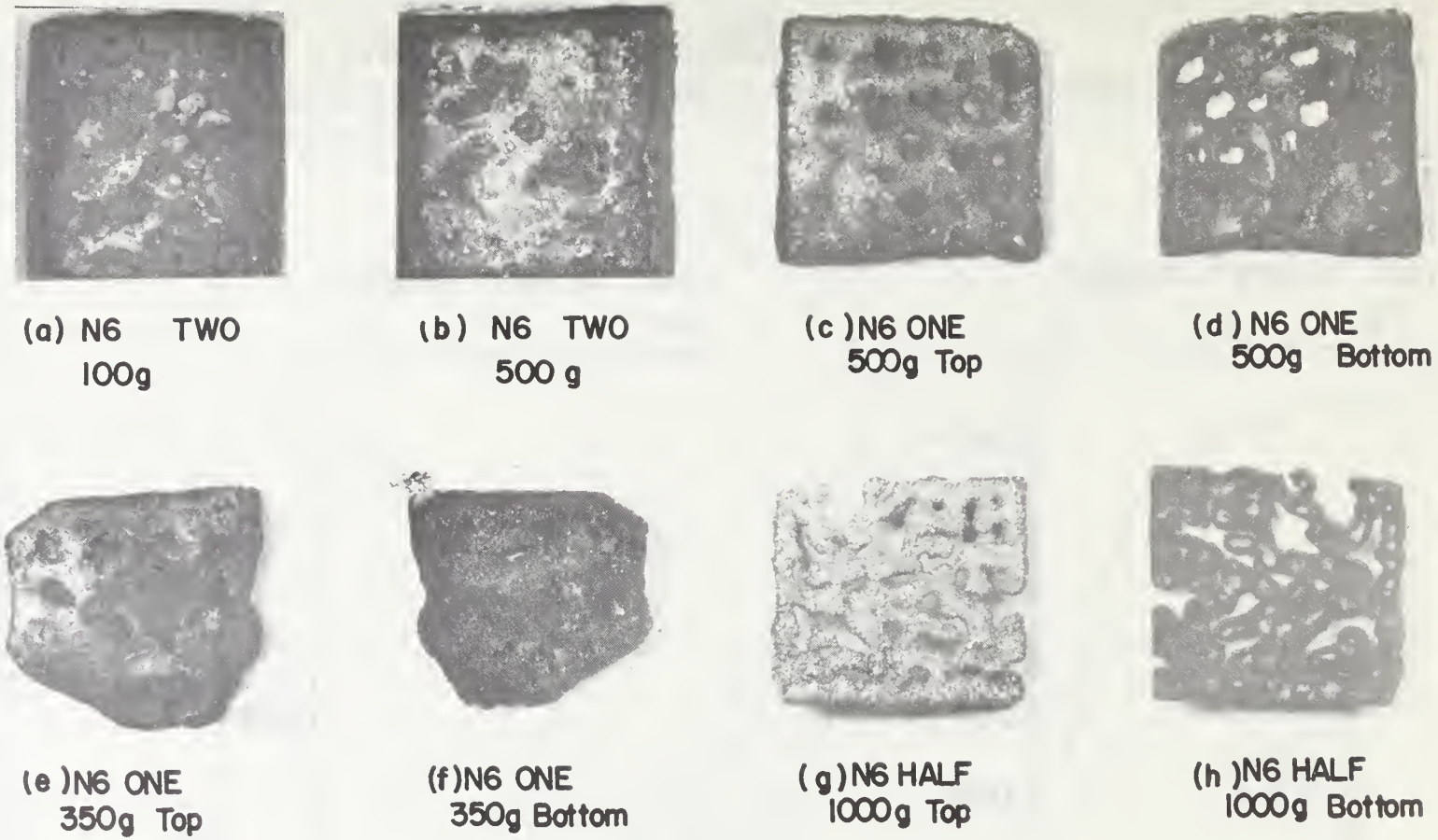

FIGURE.7. N6 TWO INCH STRAND RESIDUE AND SELECTED N6 BOTTOM VIEWING (MAG. 3X)

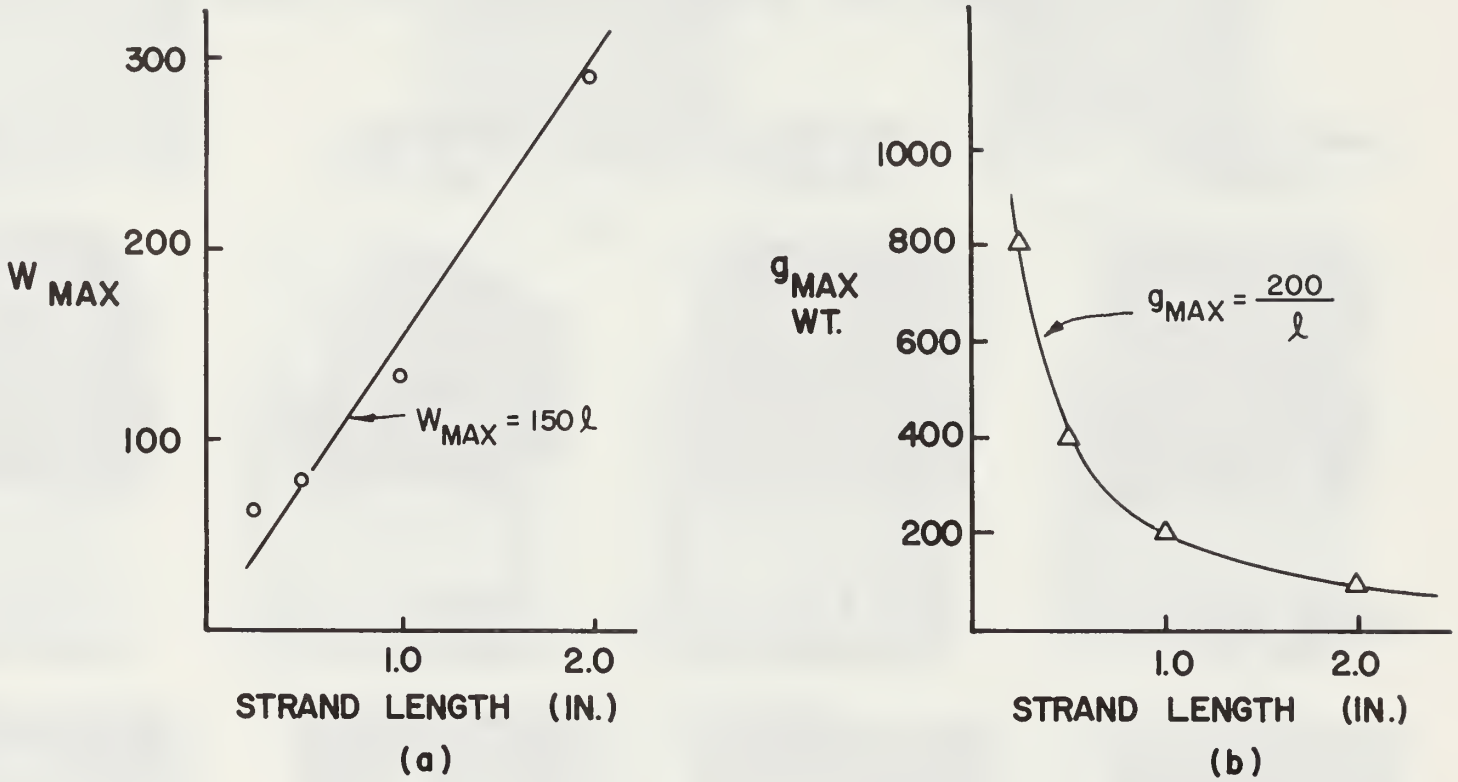

FIGURE 8. EFFECT OF STRAND LENGTH ON MAXIMUM RESIDUE WEIGHT AND ACCELERATION LEVEL FOR MAXIMUM RESIDUE WEIGHT.

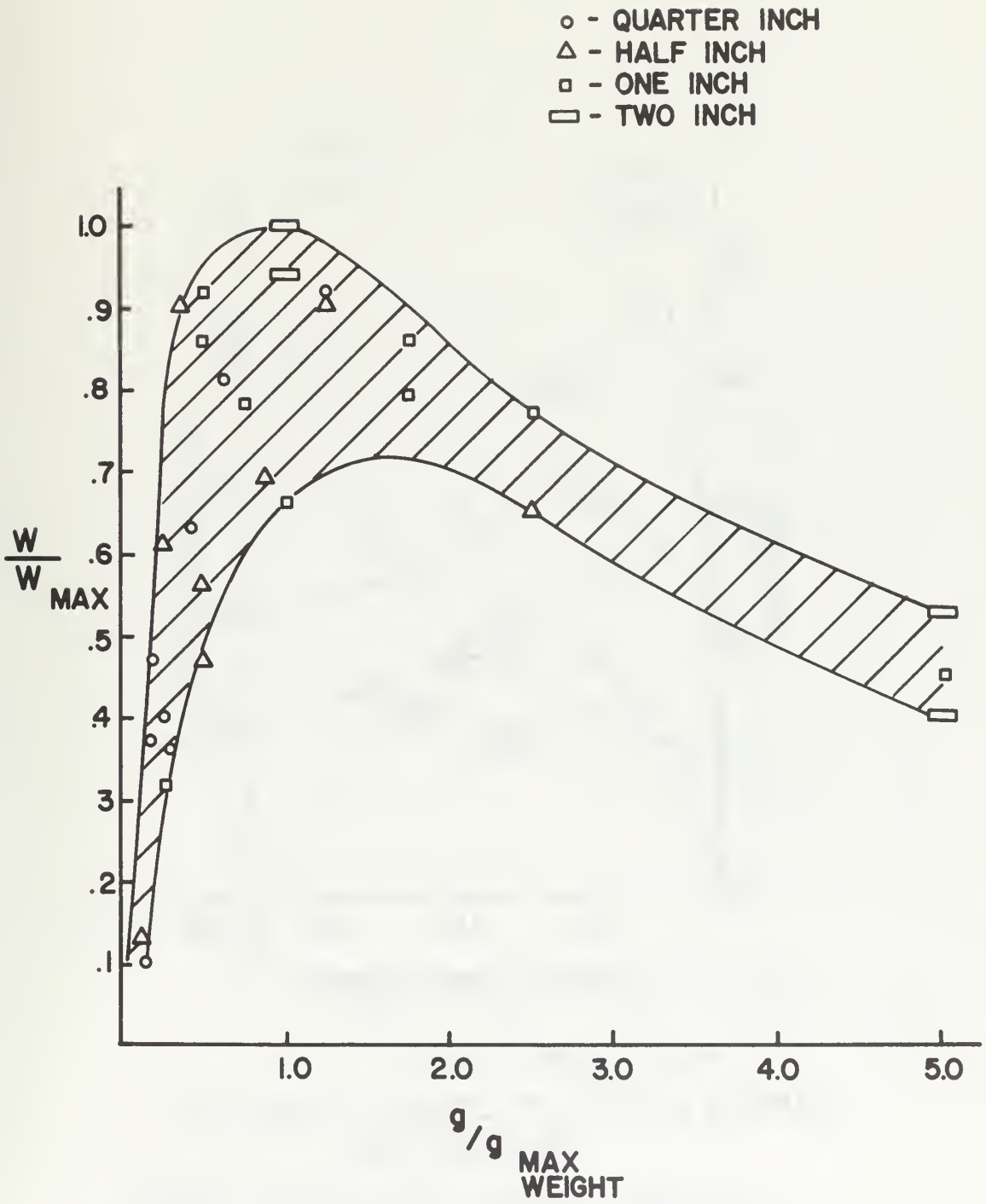

FIGURE 9. EFFECT OF ACCELERATION ON RESIDUE WEIGHT FOR PROPELLANT N6 (NORMALIZED FORM)

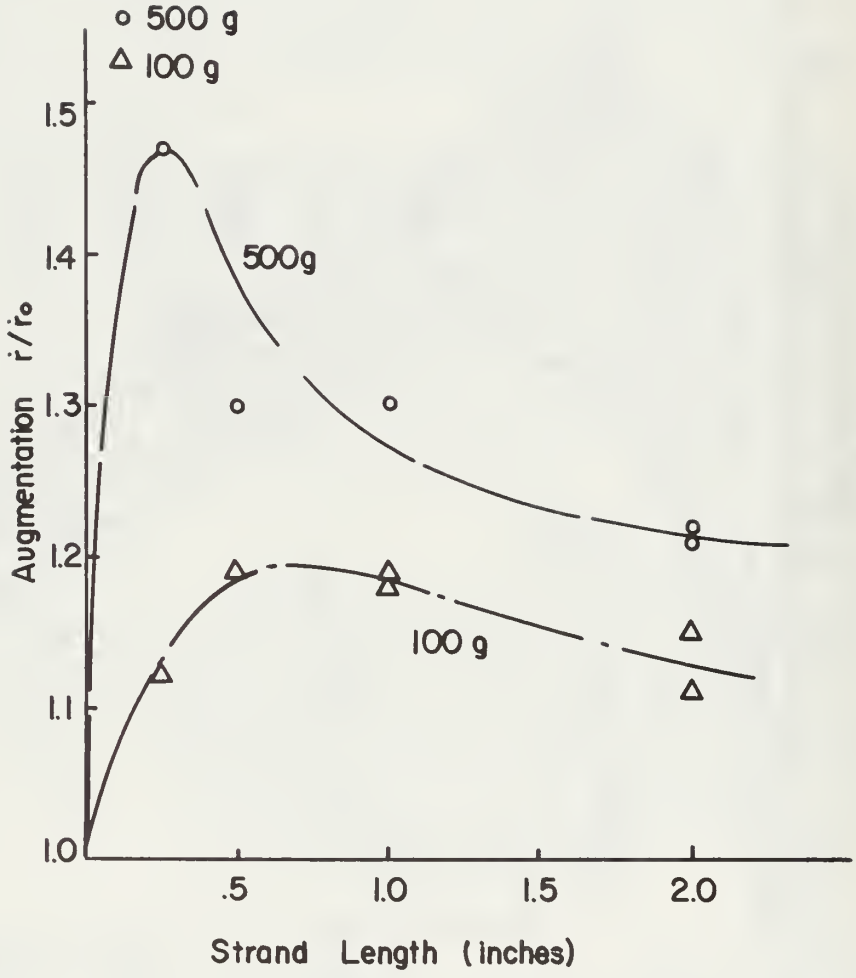

FIGURE 10. EFFECT OF STRAND LENGTH ON AUGMENTATION

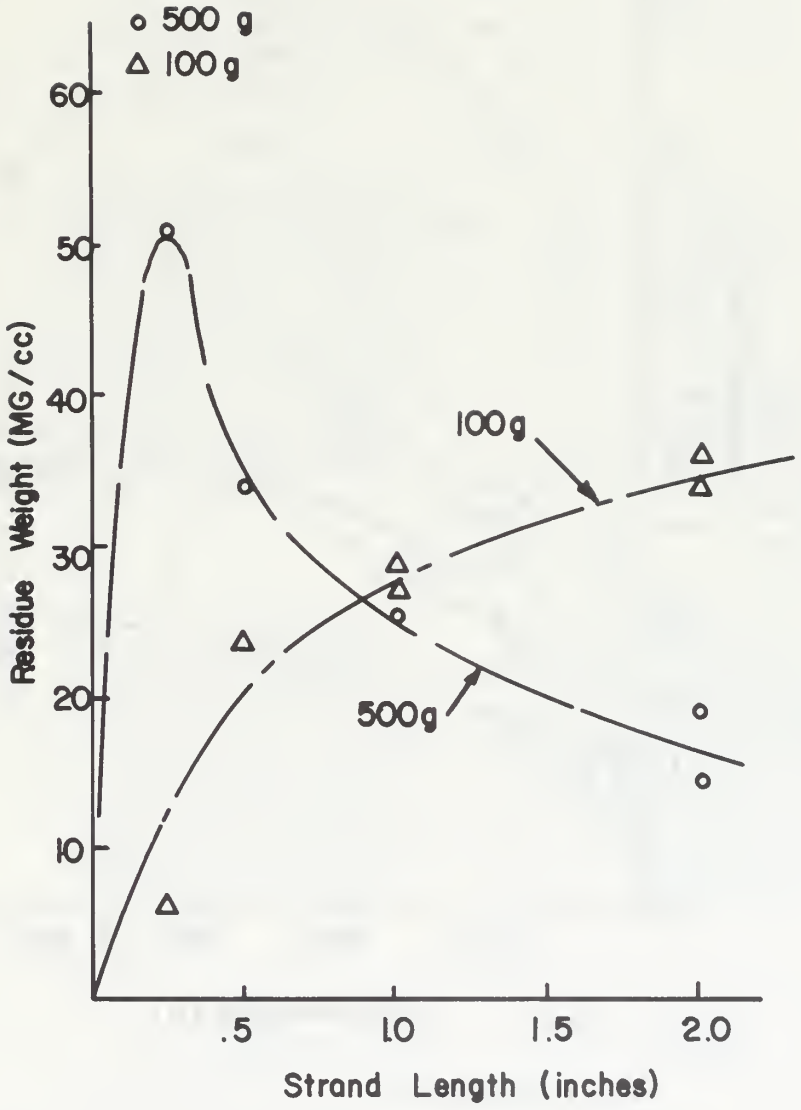

FIGURE 11. EFFECT OF STRAND LENGTH ON RESIDUE WEIGHT

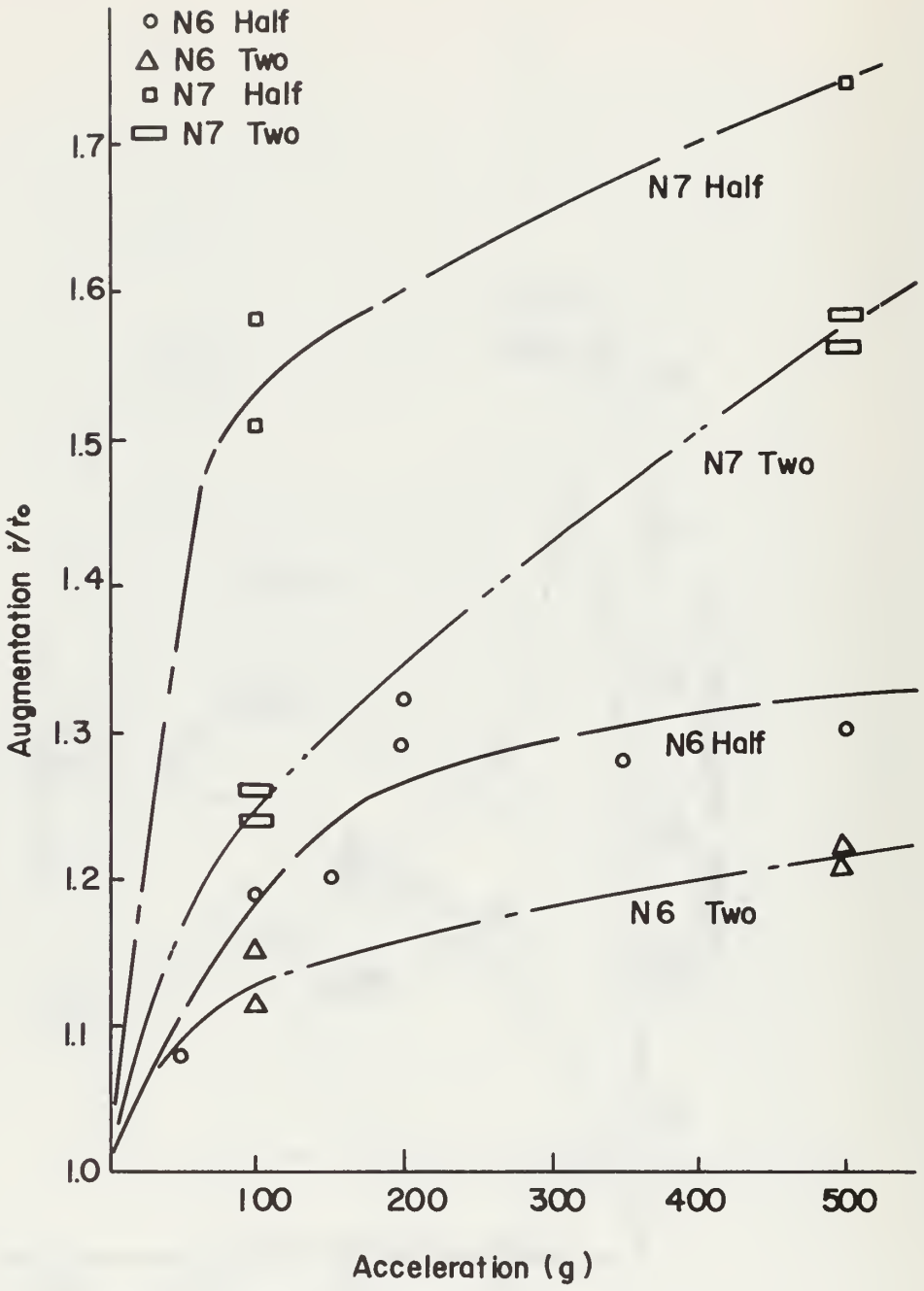

FIGURE 12. EFFECT OF BASE BURNING RATE AND AP SIZE ON AUGMENTATION

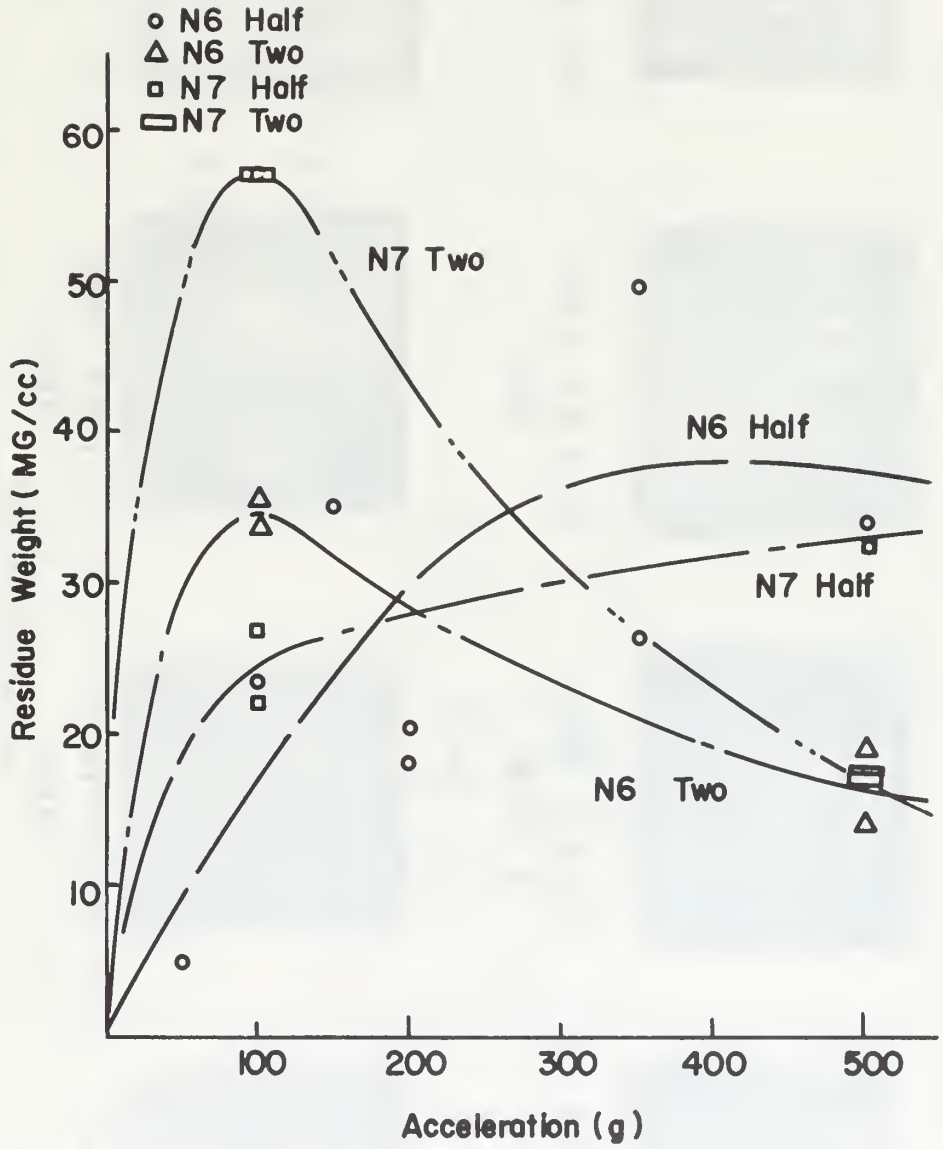

FIGURE 13 EFFECT OF BASE BURNING RATE AND AP SIZE ON RESIDUE WEIGHT

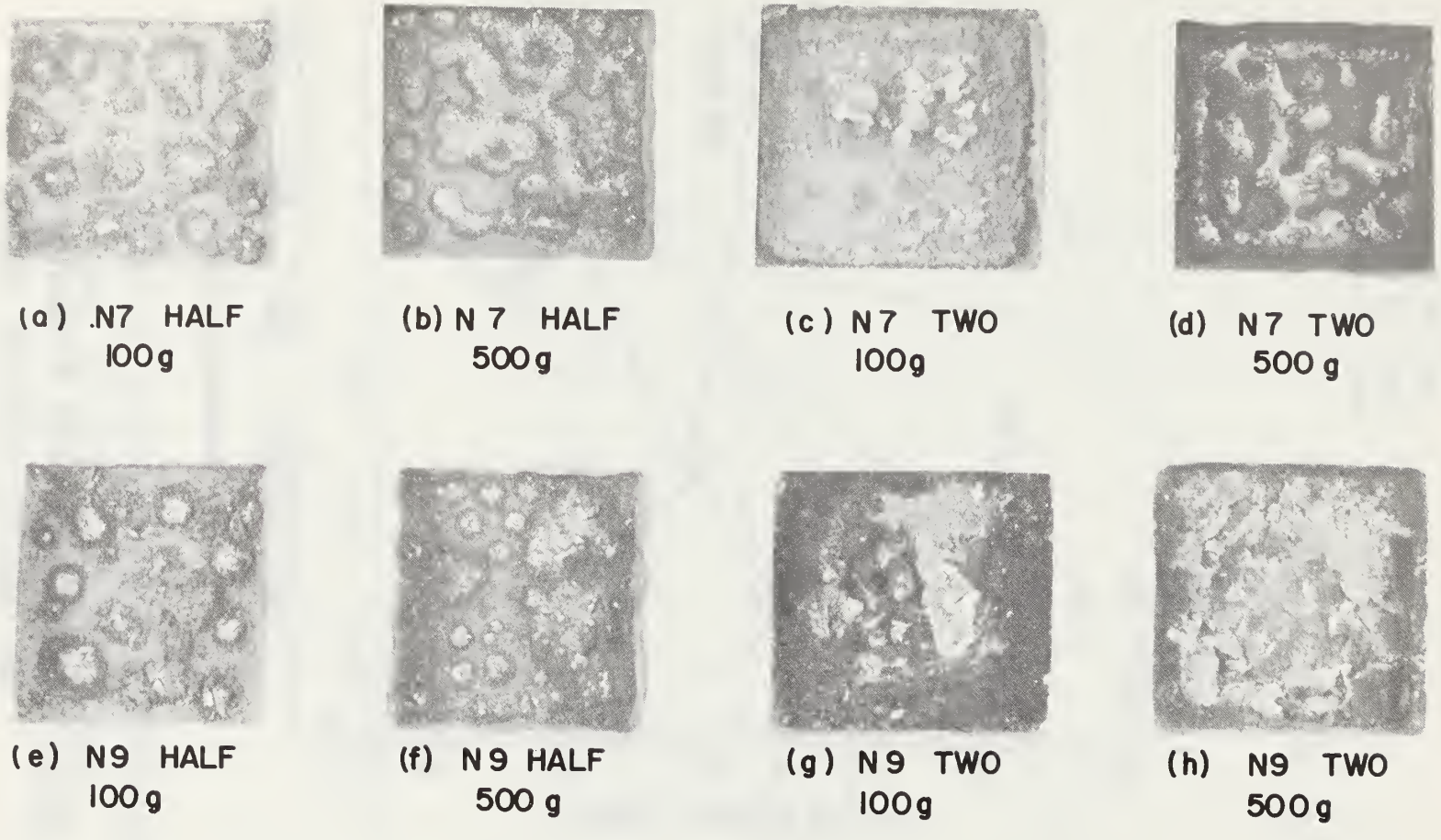

FIGURE 14. N7 AND N9 RESIDUE (MAG. 3X)

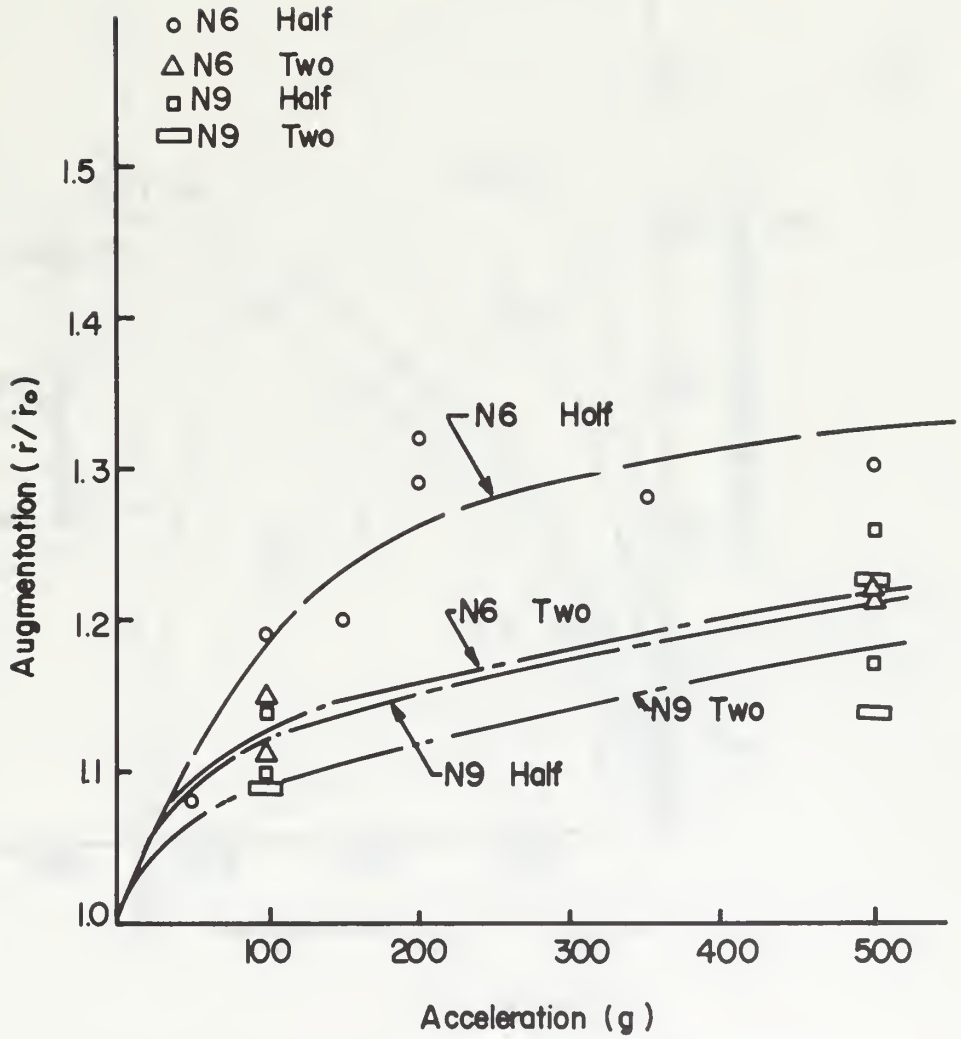

FIGURE 15. EFFECT OF AP SIZE ON AUGMENTATION

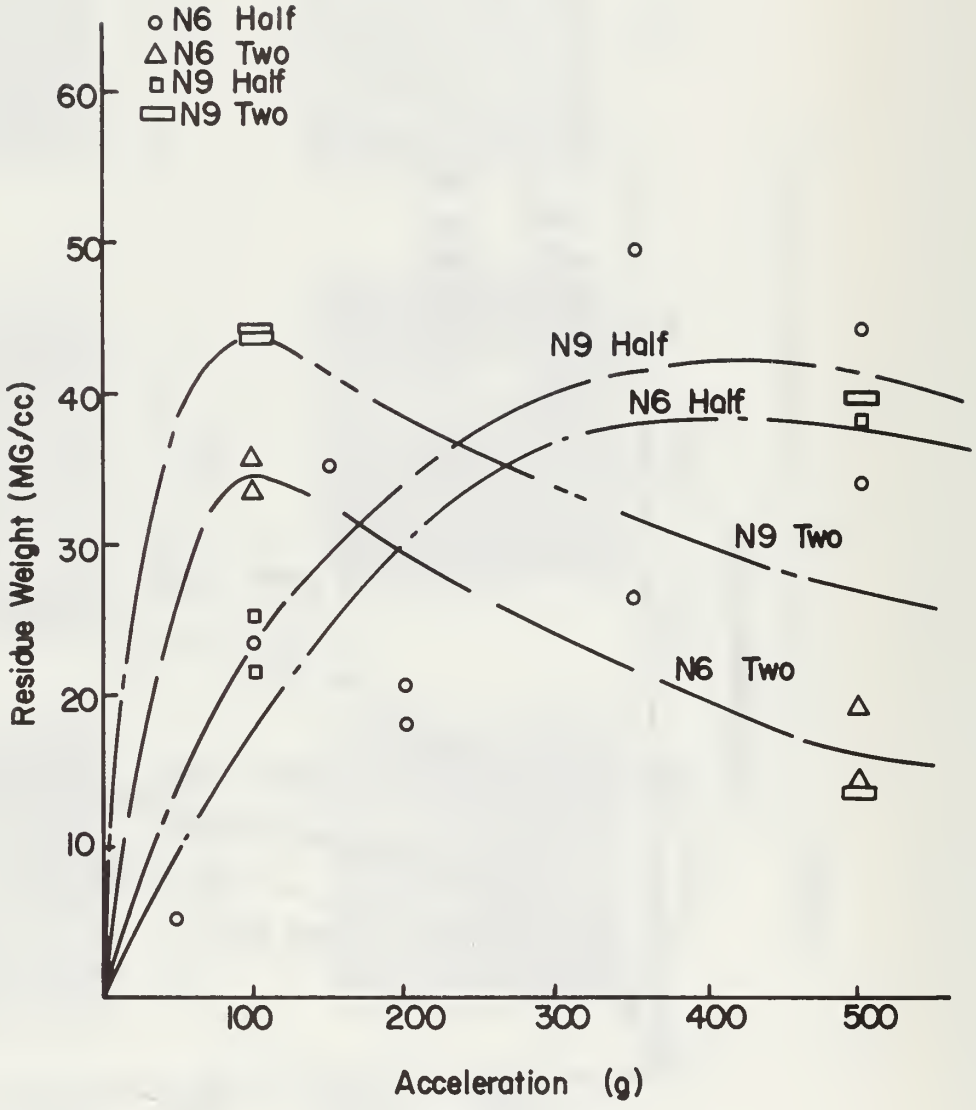

FIGURE 16. EFFECT OF AP SIZE ON VARIATION ON RESIDUE WEIGHT.

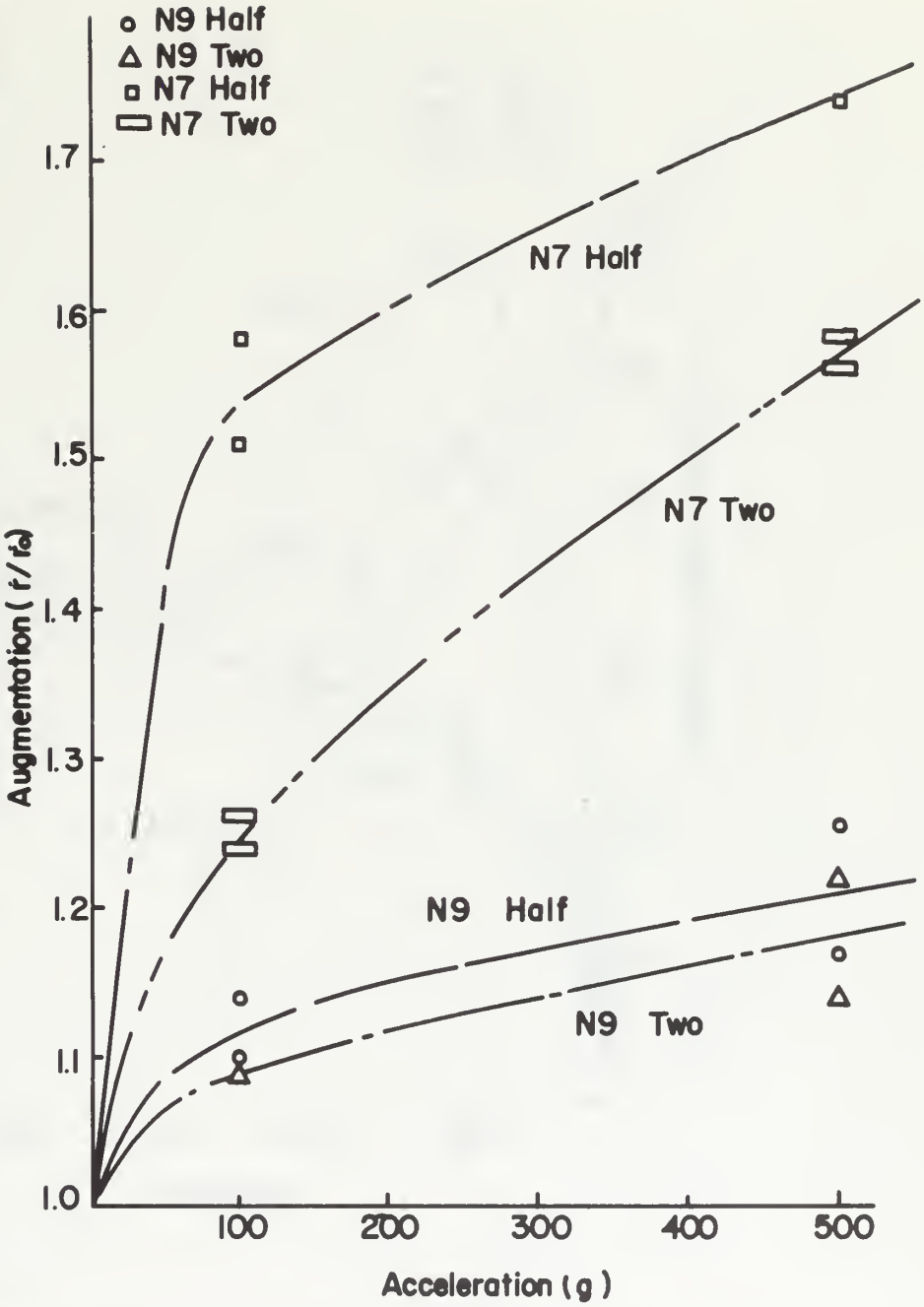

FIGURE 17. EFFECT OF BASE BURNING RATE ON AUGMENTATION

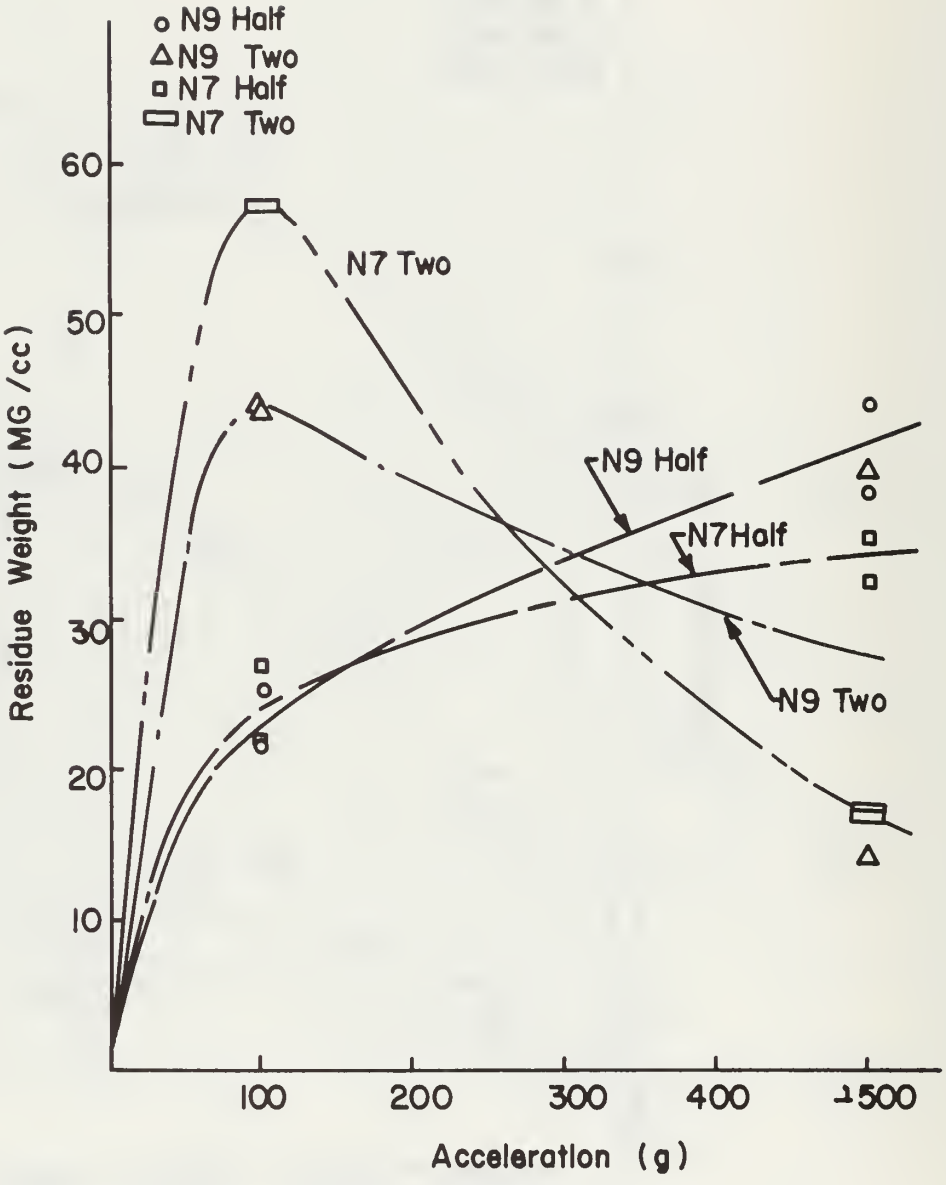

FIGURE 18. EFFECT OF BASE BURNING RATE ON RESIDUE WEIGHT

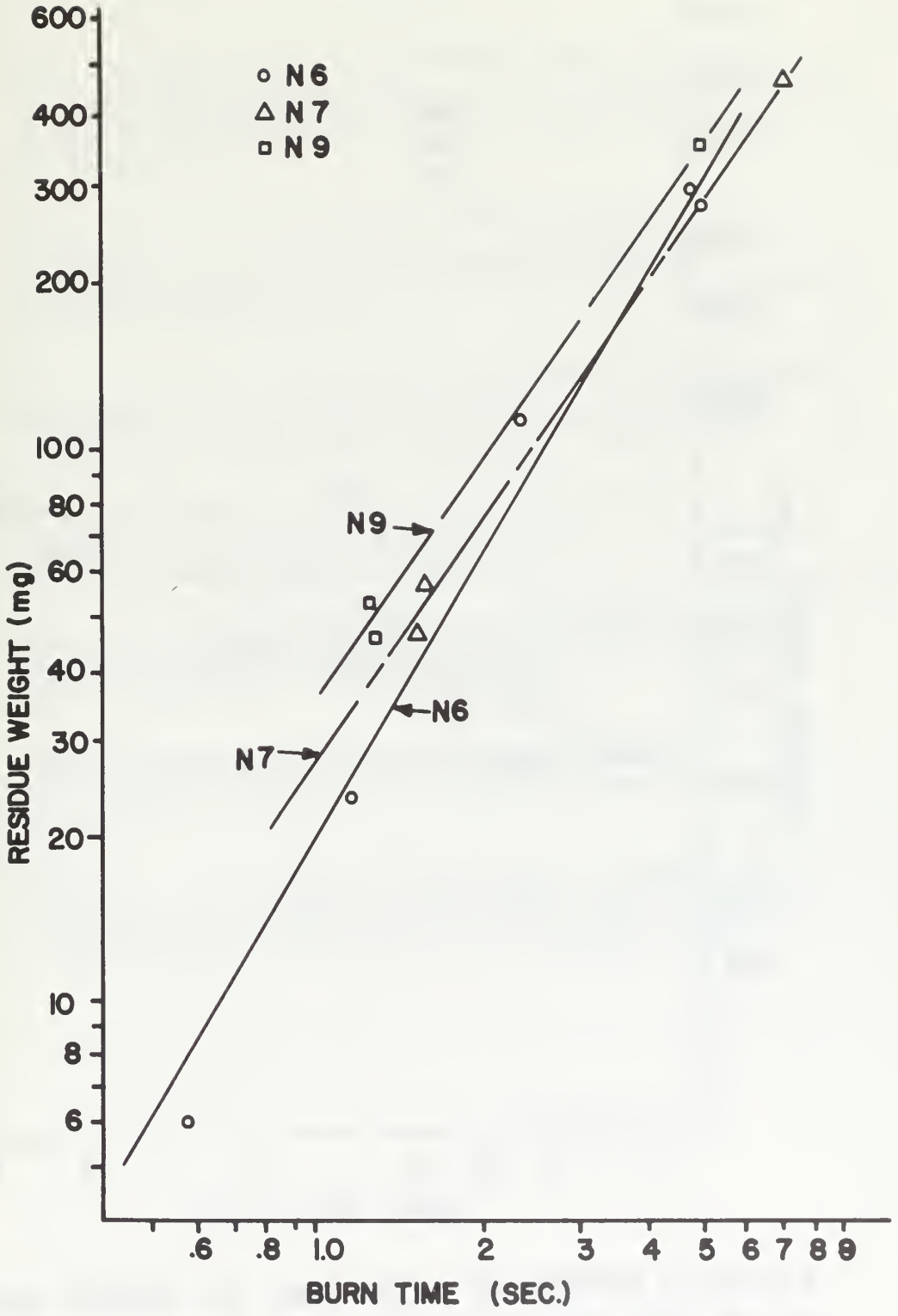

FIGURE 19. EFFECT OF BURN TIME ON RESIDUE WEIGHT OF N6, N7, N9, AT 100 g.

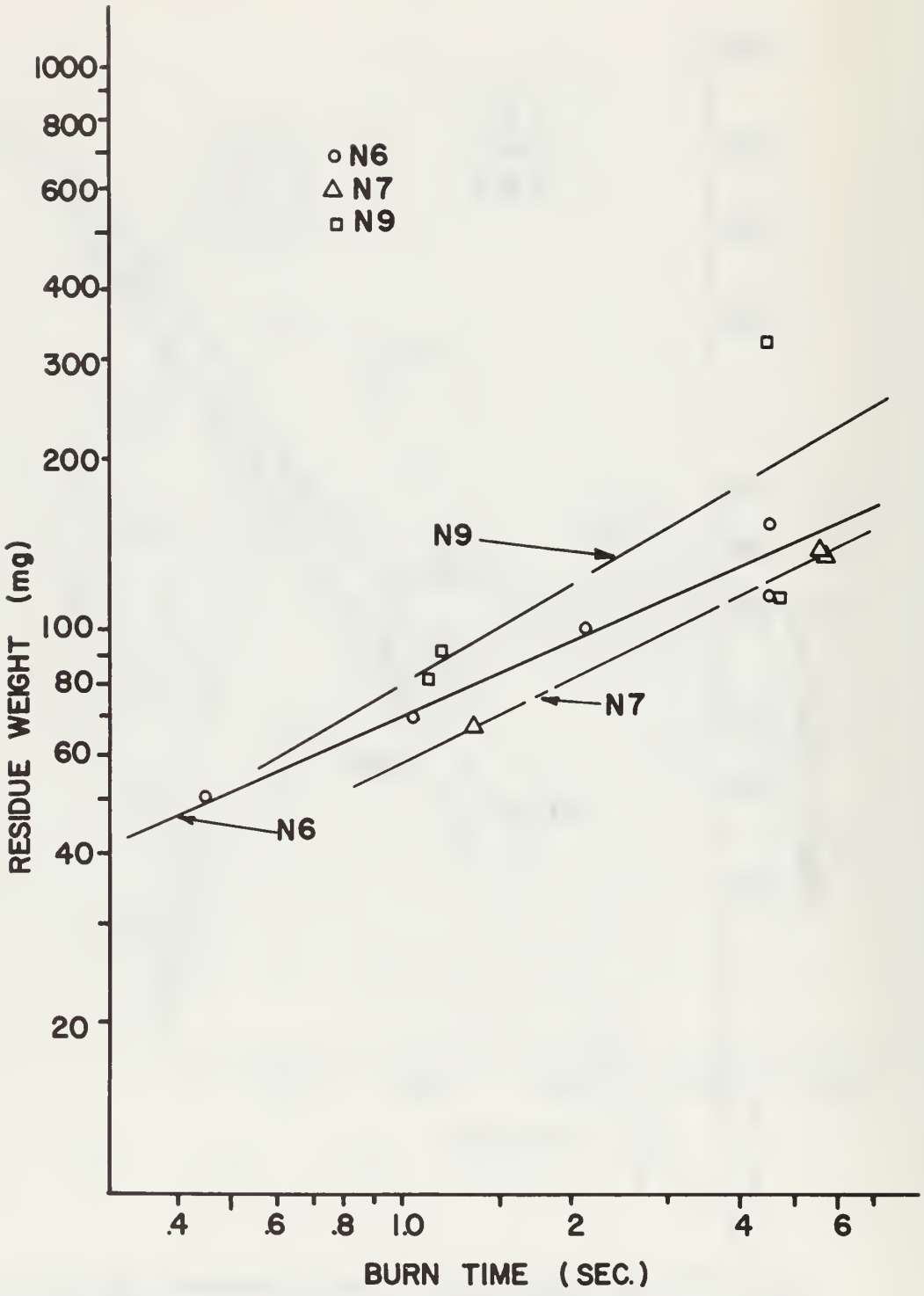

FIGURE 20. EFFECT OF BURN TIME ON RESIDUE WEIGHT OF N6, N7, N9, AT 500 g.

REFERENCES

1. Naval Postgraduate School Report NPS-57NT9101A, An Investigation of the Effects of Acceleration on the Burning Rates of Solid Propellants, by D. W. Netzer, and others, 1 October 1969.

2. United Technology Center Report NASA CR-66824, Photographic Study of Solid Propellants Burning in an Acceleration Environment, by P. G. Willoughby, K. L. Baker, and R. W. Hermsen.

3. United Technology Center Report UTC 2281-FR, Investigation of Internal Ballistic Effects in Spinning Solid Propellant Motors, P. G. Willoughby, and others, October 1968.

4. Naval Postgraduate School Technical Note TN 66T-4, 76-Inch Diameter Centrifuge Facility, by J. B. Anderson and R. E. Reichenbach, September 1966.

5. Sturm, E. J., A Study of the Burning Rates of Composite Solid Propellants in Acceleration Fields, Ph.D. Thesis, Naval Postgraduate School, March 1968.

6 Inorganic Index to the Powder Diffraction File 1968, ASTM Publication PD1S-181, American Society for Testing and Materials, 1968.

7. Northam, G. B., Effects of Steady-State Acceleration on Combustion Characteristics of an Aluminized Composite Solid Propellant, NASA TN D-4914, December 1968.

INITIAL DISTRIBUTION LIST

		No. Copies
1.	Defense Documentation Center Cameron Station Alexandria, Virginia 22314	20
2.	Library, Code 0212 Naval Postgraduate School Monterey, California 93940	2
3.	Commander, Naval Ordnance Systems Command Naval Ordnance Systems Command Headquarters Washington, D. C. 20360	1
4.	Assistant Professor D. W. Netzer, Code 57 Naval Postgraduate School Monterey, California 93940	1
5.	LCDR David E. Cowles, USN 9972 Red Rock Court San Diego, California 92131	1
6.	Chairman Department of Aeronautics Naval Postgraduate School Monterey, California 93940	1
7.	Commander, Naval Air Systems Command Navy Department Washington, D. C. 20360	1

Security Classification

DOCUMENT CONTROL DATA - R & D

(Security classification of title, body of abstract and indexing annotation must be entered when the overall report is classified)

1. ORIGINATING ACTIVITY *(Corporate author)*

Naval Postgraduate School
Monterey, California 93940

2a. REPORT SECURITY CLASSIFICATION

Unclassified

2b. GROUP

3 REPORT TITLE

An Investigation of the Effects of Acceleration and Strand Length on Post-Fire Residue of Aluminized Propellants

4. DESCRIPTIVE NOTES *(Type of report and, inclusive dates)*

Master's Thesis (April 1970)

5. AUTHOR(S) *(First name, middle initial, last name)*

David Eugene Cowles

6. REPORT DATE	7a. TOTAL NO. OF PAGES	7b. NO. OF REFS
April 1970	75	7

8a. CONTRACT OR GRANT NO.

b. PROJECT NO.

c.

d.

9a. ORIGINATOR'S REPORT NUMBER(S)

9b. OTHER REPORT NO(S) *(Any other numbers that may be assigned this report)*

10. DISTRIBUTION STATEMENT

[redacted]

11. SUPPLEMENTARY NOTES

*Approval granted only upon release by:
Naval Ordnance Systems Command.

12. SPONSORING MILITARY ACTIVITY

Naval Postgraduate School
Monterey, California

13. ABSTRACT

Aluminized propellant strand lengths from one-quarter to two inches were burned at accelerations from zero to 1000g at a mean combustion pressure of 500 psia to study the effect of acceleration and strand length on burning rate augmentation. Propellant ammonium perchlorate oxidizer size and base burning rate were varied to investigate their effects. Each post-fire residue was photographically recorded and chemical analysis was performed by X-Ray powder diffraction.

Burning rate augmentation decreased and residue weight increased when the strand length was increased. Aluminum and aluminum oxide were identified at low accelerations independent of strand length; aluminum oxide was not detectable at high accelerations. Ammonium perchlorate size and base burning rate had little effect on the functional dependence of residue weight on burn time. The Crowe, et al., model was found to indicate the correct augmentation trend as a function of burn time if the time-history of the metallic agglomerates is known.

DD FORM 1 NOV 68 1473 (PAGE 1)

S/N 0101-807-6811

Security Classification

A-31408

14 KEY WORDS	LINK A		LINK B		LINK C	
	ROLE	WT	ROLE	WT	ROLE	WT
Solid propellant						
Burning rate						
Acceleration